Schweizerische Eidgenossenschaft
Confédération suisse
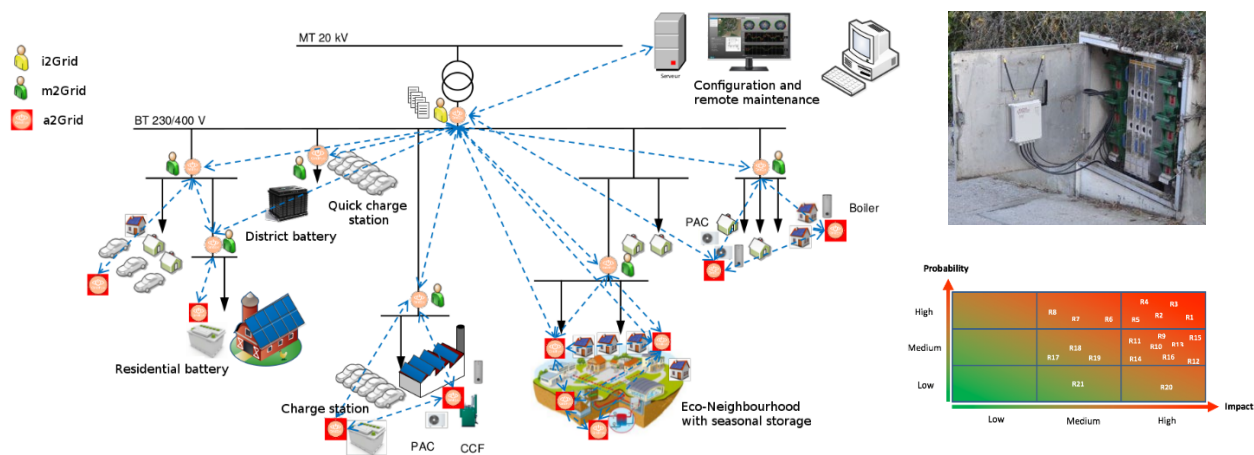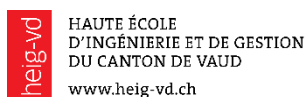Confederazione Svizzera
Confederaziun svizra

Final report

SMILE-FA

The theoretical and application **S**tudy on a Metering and Intelligent tool for Low Voltage grid control Enhancement – Flexibility Assessment

Author:
Prof. Dr. Mauro Carpita, HEIG-VD/ IESE,
Douglas Houmard, HEIG-VD/IESE,
Dr. Daniel Siemaszko, HEIG-VD/IESE,
Dr. Sébastien Wasterlain, HEIG-VD/IESE,
Dr. Mokhtar Bozorg, HEIG-VD/IESE,
Prof. Dr. Alexandre Karlov, HEIG-VD/IICT
Prof. Jean-Roland Schuler, HEIA-FR,
Joël Jaton, DEPsys SA,
Dr. Omid Alizadeh-Mousavi, DEPsys SA,
Simon Reynaud, DEPsys SA,
Antony Pinto, DEPsys SA
Jonathan Bischof, DEPsys SA.
Arnoud Bifrare, Romande Energie SA,

External partners:
Prof. Dr. Mario Paolone, EPFL/DESL,

Summary

In this project, we studied both theoretical and practical aspects related to application of low voltage grid monitoring system on grid control and flexibility assessment.

In this respect, first we improved existing methods and algorithms developed in the scope of the previous SMILE project (financed by the SFOE) regarding model-less method for computation of sensitivity coefficients of nodal voltages with respect to active and reactive power injections.

Second, we investigated the potential of distributed PV plants for providing primary voltage control to low voltage grids. The optimal control problem is formulated in such a way that it guarantees a proportionally fair scheduling of the controllable PV units. Starting from the centralized formulation of the optimal control problem, a distributed algorithm for handling over-voltages was also designed. The distributed version of the algorithm relies on a dual decomposition framework and has been shown to converge to the same solution as the centralized algorithm.

Third, we investigated the Cybersecurity protection aspects the proposed low voltage monitoring solution. During this activity, a full threat model of the system was established, a risk analysis performed and a security architecture developed. The security architecture is based on a Virtual Private Network (VPN) which provides confidentiality and integrity of information exchanged between Smart Grid devices and backend infrastructure (back-end servers). This security architecture has been successfully tested and deployed in production. A penetration test has been performed on the backend infrastructure (including web-based frontend), on the infrastructure connecting modules as well as on the modules themselves.

Forth, the methods of computation of voltage sensitivity coefficients with respect to active and reactive power injections were tested and validated under known operational conditions in the "Smart Grid – Reseaux Intelligent- ReIne" laboratory of the HEIG-VD. The results of validation test have shown that the relative differences between the sensitivity coefficients are good and testify the worthy performances of the model-less method.

Finally, we implemented and successfully tested a model-less and decentralized optimal control approach based on the estimated sensitivity coefficients, in a distribution network in Switzerland.

Résumé

Dans le cadre de ce projet, nous avons étudié les aspects théoriques et pratiques liés à l'application du système de monitoring de réseau basse tension au contrôle du réseau et à l'évaluation de la flexibilité.

À cet égard, nous avons d'abord amélioré les méthodes et les algorithmes existants, développés dans le cadre du précédent projet SMILE (financé par l'OFEN), concernant la méthode sans modèle pour le calcul des coefficients de sensibilité des tensions nodales par rapport aux injections de puissance active et réactive.

Deuxièmement, nous avons étudié le potentiel des installations photovoltaïques (PV) distribuées pour le contrôle de la tension des réseaux basse tension. Le problème de contrôle optimal est formulé de manière à garantir une répartition proportionnellement équitable de la production d'électricité entre les installations PV contrôlables. À partir de la formulation centralisée du problème de contrôle optimal, un algorithme distribué pour la gestion des surtensions a également été conçu. La version distribuée de l'algorithme est basée sur un cadre de décomposition double (doual decompostion) et il a été démontré qu'il converge vers la même solution que l'algorithme centralisé.

Troisièmement, nous avons étudié les aspects de protection contre les cyberattaques dans la solution de monitoring proposé (solution GridEye). Au cours de cette activité, un modèle de menace complet du système a été établi, une analyse de risque effectué et une architecture de sécurité développée. L'architecture de sécurité repose sur un réseau privé virtuel (VPN) qui assure la confidentialité et l'intégrité des informations échangées entre les périphériques Smart Grid et l'infrastructure back-end (serveurs principaux). Cette architecture de sécurité a été testée et déployée avec succès. Un test de pénétration a été effectué sur l'infrastructure back-end (y compris l'interface Web), sur les modules de connexion d'infrastructure ainsi que sur les modules GridEye eux-mêmes.

Les méthodes de calcul des coefficients de sensibilité de la tension par rapport des injections de puissance active et réactive ont ensuite été testées et validées dans des conditions de fonctionnement connues dans le laboratoire « Reseaux Intelligent-ReIne » de la HEIG-VD. Les résultats du test de validation ont montré que les différences relatives entre les coefficients de sensibilité sont bonnes et confirme les bonnes performances de la méthode sans modèle.

Enfin, nous avons mis en place et testé avec succès une approche de contrôle optimal sans modèle et décentralisée basée sur les coefficients de sensibilité estimés, dans un réseau de distribution réel en Suisse.

Zusammenfassung

In diesem Projekt untersuchten wir sowohl theoretische als auch praktische Aspekte im Zusammenhang mit der Anwendung von Überwachungssystemen von Niederspannungsnetze auf die Netzregelung und Flexibilitätsbewertungen.

In diesem Zusammenhang haben wir zuerst existierende Methoden und Algorithmen verbessert, die im Rahmen des vorherigem SMILE Projektes (finanziert von der BFE) zur modelllosen Methodik für die Berechnung von Sensitivitätskoeffizienten von Knotenspannungen in Bezug auf die Einspeisung von Wirk- und Blindleistung entwickelt wurden.

In einem zweiten Schritt haben wir das Potential von verteilten PV-Anlagen zur Bereitstellung der Primärspannungsregelung von Niederspannungsnetzen untersucht. Das optimale Regelungsproblem ist so formuliert, dass es eine anteilige faire Planung der steuerbaren PV-Anlagen gewährleistet. Ausgehend von der zentralisierten Formulierung des optimalen Regelungsproblems wurde auch ein dezentraler Algorithmus zum Umgang mit Überspannungen entwickelt. Die dezentrale Version des Algorithmus basiert auf einer dualen Dekompositionsmethode und konvergiert nachweislich gegen die gleiche Lösung wie der zentralisierte Algorithmus.

Drittens haben wir die Aspekte des Cybersicherheitsschutzes der vorgeschlagenen Niederspannungsüberwachungslösung untersucht. Während dieser Aktivität wurde eine vollständige Bedrohungsmodellierung des Systems erstellt, eine Risikobewertung durchgeführt und eine Sicherheitsarchitektur entwickelt. Die Sicherheitsarchitektur basiert auf einem Virtual Private Network (VPN), das die Vertraulichkeit und Integrität des Informationsaustauschs zwischen Smart Grid-Geräten und der Backend-Infrastruktur (Backend-Server) gewährleistet. Diese Sicherheitsarchitektur wurde erfolgreich getestet und in der Produktion eingesetzt. Ein Penetrationstest wurde an der Backend-Infrastruktur (inklusive webbasiertes Frontend), den Infrastrukturverbindungsmodulen sowie an den Modulen selbst durchgeführt.

Im vierten Schritt wurden die Methoden zur Berechnung von Spannungssensitivitätskoeffizienten in Bezug auf die Einspeisung von Wirk- und Blindleistung unter bekannten Betriebsbedingungen im Labor "Smart Grid - Reseaux Intelligent- ReIne" des HEIG-VD getestet und validiert. Die Ergebnisse des Validierungstests haben gezeigt, dass die relativen Unterschiede zwischen den Sensitivitätskoeffizienten gut sind und belegen die Leistungen der modelllosen Methodik.

Abschliessend haben wir einen modelllosen und dezentralen Ansatz zur optimalen Regelung auf Basis der geschätzten Sensitivitätskoeffizienten in einem Verteilungsnetz in der Schweiz implementiert und erfolgreich getestet.

Hes·so
Haute Ecole Spécialisée
de Suisse occidentale

Table of Contents

1 Introduction

Within the context energy transition and emergence of active distribution networks, increased penetration of decentralized generation leads to frequent violations of the grid operational constraints and calls for development of intelligent grid monitoring and control processes. In this project, we studied both theoretical and practical aspects related to application of low voltage grid monitoring system on grid control and flexibility assessments.

2 Goal of Project

The goal of this project is to develop and deploy voltage control algorithms for low voltage distribution grids. The algorithms are deployed in a decentralized low voltage monitoring and control tool, called GridEye, in a secure way. This goal is pursued through the following main activities:

- Improvement of the control algorithms of the low voltage networks based on the estimation of the sensitivity coefficients without model of the network.

- Testing of new algorithms in the REINE laboratory. This laboratory will allow tests to be carried out in a known environment, which is essential for the validation and performance testing of algorithms, as well as, unlike a real environment, the possibility of pushing the system to these limits without risk.

- Development of protection strategies against cyberattacks, to be tested also in the new REINE laboratory of the HEIG-VD.

3 Improvements of algorithms for control of LV grids

This section of report presents the results of activities to improve LV grid control algorithms. The result of these activities are reported in following sub-sections.

- Improvement of the estimation of the voltage sensitivity coefficients by
    - Analysis of the noise on GridEye measurements
    - Use of data filtering approach
- Fairness of control
- Utilization of different media communications

3.1 Improvement of estimation of voltage sensitivity coefficients

The linear relationship between voltage variations ($\widetilde{\Delta V}$) and real/reactive power variations ($\widetilde{\Delta P}, \widetilde{\Delta Q}$), is given by (1). In this equation, the voltage sensitivity coefficients with respect to real and reactive power are named K_{vp} and K_{vq}, respectively.

$$\widetilde{\Delta V} = K_{vp}\widetilde{\Delta P} + K_{vq}\widetilde{\Delta Q} \tag{1}$$

In the context of SMILE project, a method to estimate the voltage sensitivity coefficients based on the Generalized Least Square (GLS) approach has been developed [1]. Although the method most of the time is very effective, sometimes large deviations between the estimated and the actual sensitivity coefficients are observed. To face this problem, initially the assumption of the normal noise on the measurement data is examined. Then, a data filtering approach is investigated to improve the estimation of sensitivity coefficients.

3.1.1 Analysis of noise on GridEye measurements

In this sub-section, the noises of GridEye's voltage and current measurements are analysed. The values of voltages and currents are read from the corresponding sensors without measuring any current or voltage. Figure 1 shows the normal Q-Q plots and the histograms for the measured voltage and current noises. The noise of the voltage is not Normal whereas the noise of the current shows a Normal distribution.
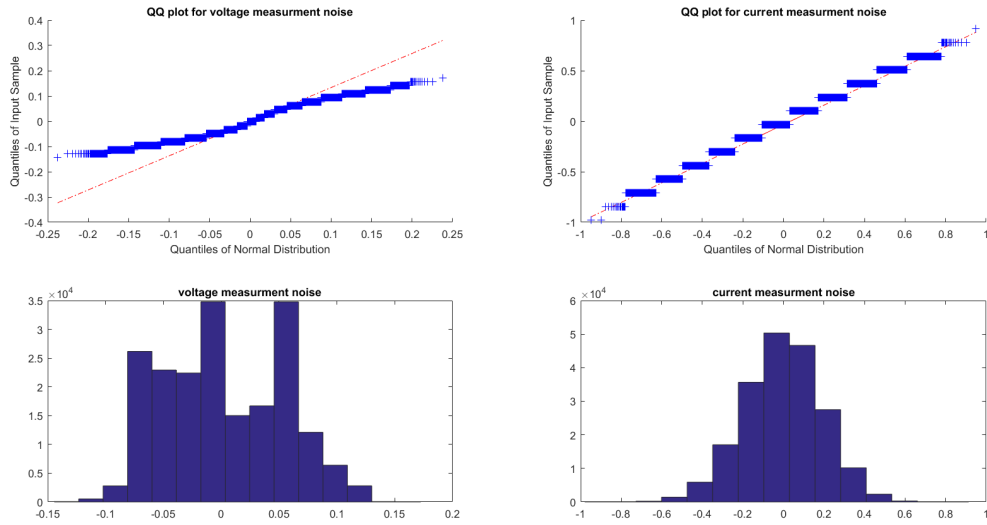
Figure 1. left) raw voltage noise data is not normal, right) raw current noise data is normal.

The measured noises are added to the perfect sinusoidal voltage and current signals, and then the RMS values are calculated for the perfect and noisy signals. The errors are assessed as the difference between the RMS values of the perfect sinusoidal and noisy signals. Similarly, the active power and its error is calculated for the perfect sinusoidal and noisy signals. The normal Q-Q plots and the histograms for the errors in voltage, current, and active power are given in Figure 2. These errors demonstrate Normal distribution behaviour. This characteristic of errors allows using GLS approach for the estimation of sensitivity coefficients.
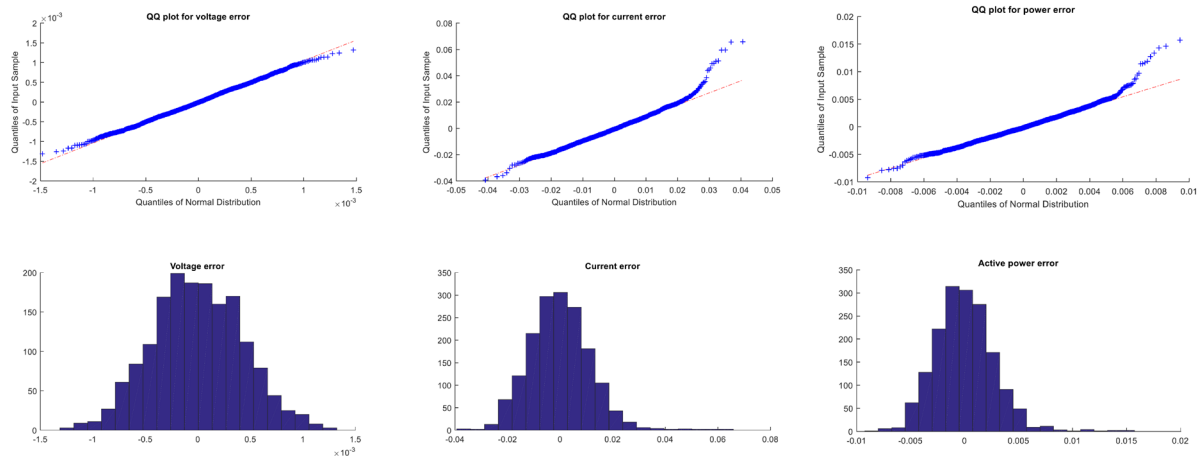
Figure 2. left) RMS voltage error is normal, center) RMS current error is almost normal, right) active power error is almost normal.

3.1.2 Data filtering approach

The data filtering approach is based on the fact that the sensitivity coefficients can be better estimated using GLS whenever there are enough variations in the measurement data. A set of measurements is considered suitable for the estimation of the voltage sensitivity coefficients if the amount of variation of the active and reactive power at each measuring node is large enough. This condition ensures that the voltage sensitivity coefficients can be properly estimated using the measurements. The amounts of

variation of the active and of the reactive power can be assessed by computing the standard deviations of the timestamped active power and reactive power values for a predefined time window. For instance, the measurements can be considered suitable if the standard deviations of the active and reactive powers are larger than a predefined threshold value. The predefined threshold value can be selected, for example, to be equal to 10% of the absolute value of the corresponding mean, and preferably to be equal to 20% of the absolute value of the corresponding mean. In the case where the measurements are not suitable for the estimation, a replacement set of data is acquired during a new time window.

The data filtering approach is used to estimate the sensitivity coefficients of a 3-bus LV grid using actual measurements for the power injections provided by GridEye and a 2000-samples time window. The voltage sensitivity coefficients of node 2 and node 3 with respect to active power changes of other nodes are shown in *Figure 3*. The theoretical sensitivity coefficients are given in blue and its ±10%, ±20%, and ±50% margins are given in dashed lines. The estimated sensitivity coefficients are illustrated by red circles. It is worth noting that the sensitivity coefficients are estimated whenever there are enough variations in the measurement data. The data filtering approach provides prominent results for the estimation of sensitivity coefficients. The integration of this point into the previously filled European patent [2] has resulted in an important improvement for the estimation of the sensitivity coefficients method. This results into the application of a Worldwide patent [3].
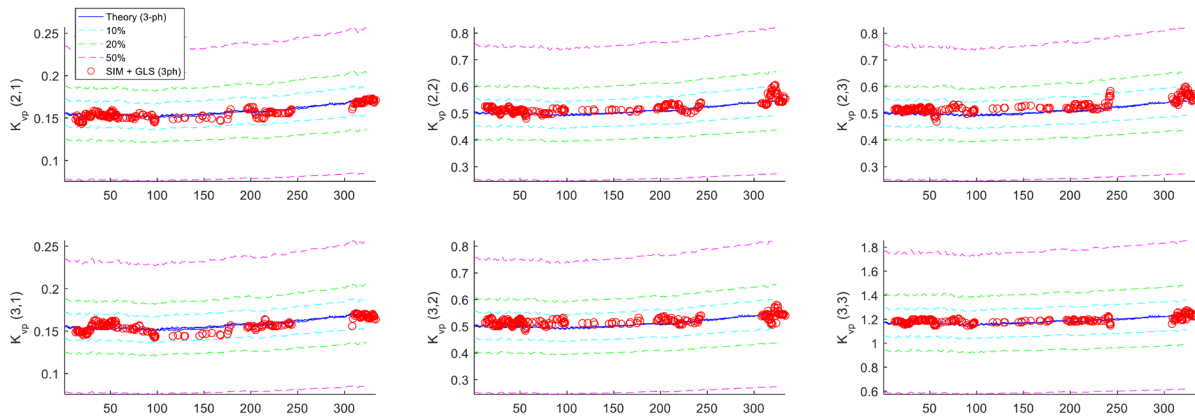

Figure 3 Comparison between the calculated (i.e. theoretical) and the estimated voltage sensitivity coefficients using data filtering approach for 3-bus system at bus 2 and 3 w.r.t. active power changes at other nodes.

3.2 Fairness of control

In this section, we evaluate the potential of distributed photovoltaic (PV) plants for providing primary voltage control to the local distribution grid. In this respect, we control the active and reactive power injections of distributed solar panels for providing primary voltage control to low voltage grids hosting significant amount of these type distributed generators. In this respect, the control scheme is designed to deal with voltage fluctuations produced by either stochastic power injections of kW-class distributed solar plants as well as large variations of loads (e.g., produced by inrushes and/or disconnections of large loads). Compared to existing schemes in the literature, we design a control algorithm for the scheduling of the solar plants using the concept of fairness. In particular, the optimal control problem is formulated in such a way that it guarantees a proportionally fair scheduling of the controllable PV units while maintaining a voltage profile within allowed limits for safe operation. Additionally, we provide both a centralized formulation of the optimal control problem, as well as a distributed version. Starting from the centralized formulation of the optimal control problem, we rely on a dual decomposition framework

to decompose the problem such that each controllable resource can update independently its power injections receiving a control signal from a master controller. The distributed version of the algorithm has been shown to converge to the same solution as the centralized algorithm.

The rest of this section is organized as follows. Section 3.2.1 introduces the formulation of the optimal control problem as well as the centralized and distributed versions of its solution. In Section 3.2.2 we evaluate the performance of the proposed algorithms through several application examples using the CIGRE LV benchmark grid [4]. Finally, Section 3.2.4 concludes this study with the main observations.

3.2.1 Problem Formulation

In this Section, we first present the centralized control problem and then a distributed version based on a dual decomposition of the optimal control problem. In the rest of this section, we consider a balanced radial network composed of M buses, a set $\mathcal{G}$ of controllable generators (in this case, solar panels) and L loads. The network admittance matrix is denoted by Y. The phase-to-ground voltage phasor of the $i-th$ node is denoted by $\bar{E}_i$ and the active and reactive nodal power injections of node i by P_i and Q_i respectively. We rely on the following hypotheses for the formulation of the problem:

H1. We consider the direct sequence representation of the grid;[1]

H2. We assume a perfect knowledge of the system parameters, i.e., the network admittance matrix;

H3. The nodal-power injections are voltage-independent;

H4. At each control time-step, the grid operation system observes the state of the grid, for instance via a state estimation algorithm.

Centralized optimal control problem

We are interested in maximizing the welfare of the prosumers that use the grid, while maintaining an acceptable network quality of service represented by the voltage profile. Specifically, we maintain the network phase-to-ground voltage amplitudes within acceptable limits by controlling the active and reactive power variations of distributed controllable devices $\mathcal{G}$ in a fair way. In our case, we assume that these devices are solely composed by distributed PV plants. Each controllable device $g \in \mathcal{G}$ has a certain utility function $U_g(.)$, and the sum of these utility functions is maximized subject to the satisfaction of the network operation constraints (voltage limits) and the capability curves of the controllable resources. The resulting set-point is thus such that no single device can increase its utility without decreasing the utility of some others, and locally-fair, i.e., the resulting set-point is a local maximizer of the sum of the device utilities lying on the Pareto boundary of feasible set-points. Such a design principle is largely adopted in TCP/IP for fair rate allocation (e.g., [5]).

The actual formulation of the optimal control problem is based on a linearization of the AC power flow equations realized via the well-known concept of voltage sensitivity coefficients. The control variables of the optimization problem are the active and reactive variations of the distributed PV panels, i.e., $\{\Delta(\boldsymbol{P}, \boldsymbol{Q})^*\}$. At each time-step t a global observer has the knowledge of the state of the network on every bus i, i.e., the per-bus aggregate power injections P_i and Q_i, along with the phasors of the phase-to-ground voltages $\bar{E}_i$.[2] Subsequently, this global observer computes the voltage sensitivity coefficients with respect to the nodal power of the buses $g \in \mathcal{G}$, where controllable resources are connected

---

[1] We have considered the direct sequence only for sake of clarity. The control problem can be easily extended to three phase unbalanced and unsymmetrical systems by using the generic computation of the voltage sensitivty coefficients proposed in [6].

[2] As discussed the the recent literature, a fundamental step towards the development of optimal control schemes for ADNs is the knowledge of the system state. To this end, we assume that the global observer is composed by a state estimation (SE) module that process field measurements and provide the DSO with the state of the grid, i.e., the voltage phasors at the network buses. It is worth noting that control

$$K_{P,ig} := \frac{\partial |\bar{E}_\imath|}{\partial P_g}, K_{Q,ig} := \frac{\partial |\bar{E}_\imath|}{\partial Q_g} \qquad (2)$$

The above sensitivity coefficients can be computed in several ways. Since we are formulating a control problem to be solved in real time, and we assume to have available a RTSE, the method we adopted relies on the solution of the linear systems of equations presented in [6]. Therefore, the following linear relation between variation in bus voltages and variations of active/reactive power ΔP_g, ΔQ_g can be derived[3]:

$$\Delta |\bar{E}_\imath| \approx \sum_{g \in G} K_{P,ig} \Delta P_g + K_{Q,ig} \Delta Q_g \qquad (3)$$

Therefore, the optimal control problem is formulated as a constrained optimization problem as follows:

$$\max_{\Delta(\boldsymbol{P},\boldsymbol{Q})} \sum_{g \in G} U_g (P_g + \Delta P_g) \qquad (4)$$

Subject to:
$$(P_g + \Delta P_g, Q_g + \Delta Q_g) \in \mathcal{H}_g, \quad \forall g \qquad (5)$$

$$\bar{E}_\imath + \sum_{g \in G} K_{P,ig} \Delta P_g + K_{Q,ig} \Delta Q_g \leq E_{\max} \quad \forall i \qquad (6)$$

where the constraints in ((5) represent the capability curves $\mathcal{H}$ of each controllable resource g, and inequality ((6) imposes a maximum allowed voltage limit.[4] In order to control the distributed generators in a fair way as mentioned above, we select the utility function of each PV plant to be a concave increasing function of the active power injection and, in particular, a logarithmic one, i.e., $U(x) = log(x)$.[5]

Distributed control algorithm

Following the methodology developed in [7] we can solve (4)-(6) in a distributed manner via a dual decomposition of the original control problem. We start by formulating the Lagrangian of the problem in (4)-(6):

$$\max_{\Delta(\boldsymbol{P},\boldsymbol{Q})} \sum_{g \in G} U_g (P_g + \Delta P_g) - \sum_i \lambda_i \left[\sum_{g \in G} K_{P,ig} \Delta P_g + K_{Q,ig} \Delta Q_g - (\bar{E}_\imath - E_{max}) \right] \qquad (7)$$

Subject to:
$$(P_g + \Delta P_g, Q_g + \Delta Q_g) \in \mathcal{H}_g, \quad \forall g \qquad (8)$$

where λ_i the Lagrange multipliers associated with inequality (6). Note that changing the order of summation in the second term of the Lagrangian (7) allows to decompose the problem at each node where a controllable resource is connected. In particular, each node $g \in \mathcal{G}$ solves independently the following optimization problem for fixed values of the Lagrange multipliers:

---

functionalities in distribution systems can be characterized by dynamics in the order of few seconds, since they might be associated to the dynamics of renewable energy resources (RERs) (e.g., [19]). In this respect, we consider the presence of a real-time state estimator (RTSE) capable of assessing the ADNs' state within few tens/hundreds of milliseconds with relatively high levels of accuracy and refresh rate (e.g., [15]).

[3] The optimal control problem is essentially a linearization of a full AC optimal power flow (OPF) problem and, therefore, constitutes a convex approximation to the original full AC-OPF problem. However, a numerical comparison between the full AC-OPF problem and its linearized version was performed off-line and it has been found that the solutions obtained are very similar, with a difference in the order of 10^{-3} p.u. .

[4] Note that only upper voltage limits are considered in the constraints. This is due to the fact that, in this work, we control distributed solar panels and therefore we can only curtail their power production to avoid overvoltages. However, this is not a limiting factor of the proposed method. Indeed, when demand response and/or distributed storage systems are included in the control, undervoltages can be taken into account in a similar way.

[5] It is worth noting that the optimal control problem in (4)-(6) is a convex problem, as it consists in the maximization of a concave objective subject to linear constraints. It this respect, we are also assuming that the capability curves $\mathcal{H}_g$ are convex sets.

Hes·so
Haute Ecole Spécialisée
de Suisse occidentale

$$\max_{\Delta(P_g, Q_g)} U_g (P_g + \Delta P_g) - \sum_i \lambda_i \left[K_{P,ig} \Delta P_g + K_{Q,ig} \Delta Q_g - (\bar{E}_\iota - E_{max}) \right] \tag{9}$$

Subject to:
$$\left(P_g + \Delta P_g, Q_g + \Delta Q_g \right) \in \mathcal{H}_g \tag{10}$$

Then, we get a centralized master problem responsible for updating the Lagrange multipliers by performing one step of gradient descent towards the solution of the following optimization problem (dual problem):

$$\min_{\lambda} f(\lambda) = \sum_i f_i(\lambda) + \lambda^T (\bar{E}_\iota - E_{max}) \tag{11}$$

Subject to:
$$\lambda \geq 0 \tag{12}$$

where $f_i(\lambda)$ is the dual function obtained as the maximum value of the Lagrangian solved in (4) for a given subproblem. The Lagrange multipliers for each network bus are updated in this case using gradient-descent for the solution of the problem in (11)-(12):

$$\lambda_i^{k+1} = \max \left(\left[\lambda_i^k - \gamma \left((\bar{E}_\iota - E_{max}) - (\sum_{g \in G} K_{P,ig} \Delta P_g + K_{Q,ig} \Delta Q_g) \right) \right], 0 \right) \tag{13}$$

where γ is the step size. The distributed algorithm is described Algorithm 1 below, and is schematically illustrated in *Figure 4*. The entire algorithm is run at every control time step t. In what follows we evaluate the performances of both algorithms and we show that the distributed algorithm converges to the same solution as the centralized one.

Algorithm 1 Distributed algorithm for the solution of the problem in (4)-(6)

- At each time step set iteration index $k = 0$ and initialize control variables $\Delta P_g^0, \Delta Q_g^0$ and Lagrange multipliers λ_i^0
1) **Repeat**
2) Each generator $g \in \mathcal{G}$ obtains optimal $\Delta P_g^{k*}, \Delta Q_g^{k*}$ by solving problem (9)-(10) for fixed $\lambda = \lambda^k$ and sends the optimal solution to the master controller.
3) The master controller updates the Lagrange multipliers using the expression in (9) and transmits the new values to the controllable generators.
4) Set $k \leftarrow k + 1$
5) **Until** the maximum number of iterations has been reached **or** the change in the Lagrange multipliers and the control variables between two consecutive iterations is less than a tolerance $\delta > 0$
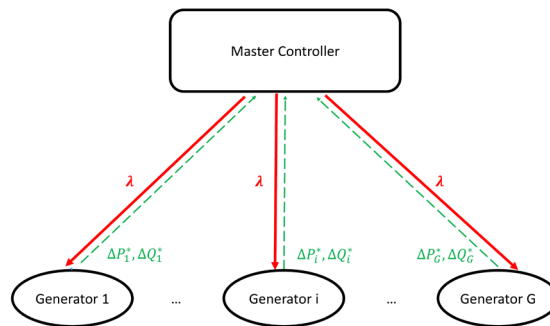

Figure 4 Distributed control algorithm

3.2.2 Application examples

Simulation settings

For the evaluation of the proposed mechanism we use the CIGRE LV benchmark grid described in [4]. The network topology, composed of 18 nodes, is shown in Figure 5. The primary substation transformer is taken into account by considering its short-circuit internal impedance. The base value of the network voltage is 400 V.
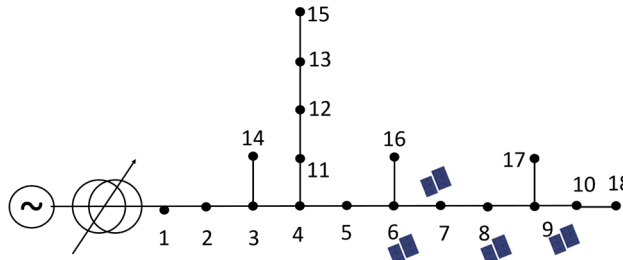

Figure 5 Topology of CIGRE LV benchmark grid.

The load of each network bus is represented by typical 24hr curves inferred from real measurements. The aggregate consumption of the feeder is shown in *Figure 6 - left*. Concerning the controllable resources, we assume distributed PV sources connected to buses 6, 7, 8 and 9 (see *Figure 5*). The aggregate generation profile of the grid is shown in the *Figure 6 - right*. As it can be seen, the scenario we are using is intentionally build in a way that the PV generation peak is in the order of two times larger the peak demand.
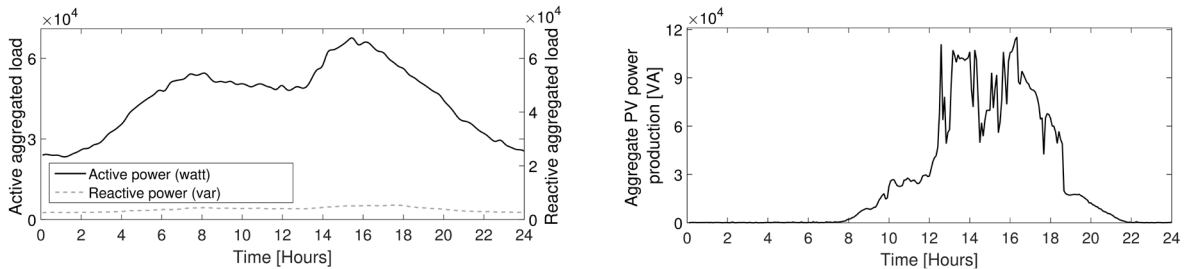

Figure 6 **left**) aggregate load, **right**) Aggregate PV production.

We consider three test cases:

1) Case 0 (base case): no control is activated and the PV sources are allowed to produce their maximum possible power following, for instance, a maximum power point tracking control. The power factor of the devices is set to 1, therefore no reactive power support is provided.

2) Case 1: the centralized control of the PV sources is activated and the problem (4)-(6) is solved using a built-in Matlab solver based on an active-set algorithm.

3) Case 2: the distributed Algorithm 1 is implemented to schedule the power production of the PV sources.

3.2.3 Evaluation of the proposed algorithms

We first evaluate the performance of the proposed algorithms with respect to the optimality of the voltage control. *Figure 7* (a) below shows the minimum and maximum network voltage profiles for case 0 (base case) without any control. It can be observed that, without any control, the maximum allowed voltage

limit of 1.05 p.u. is violated multiple times in the middle of the day, during the peak PV production period. *Figure 7* (b) shows the minimum and maximum network voltage profiles for case 1, after the application of the centralized control algorithm. In this case the control can maintain the network voltages throughout the day within the acceptable limits for safe operation.
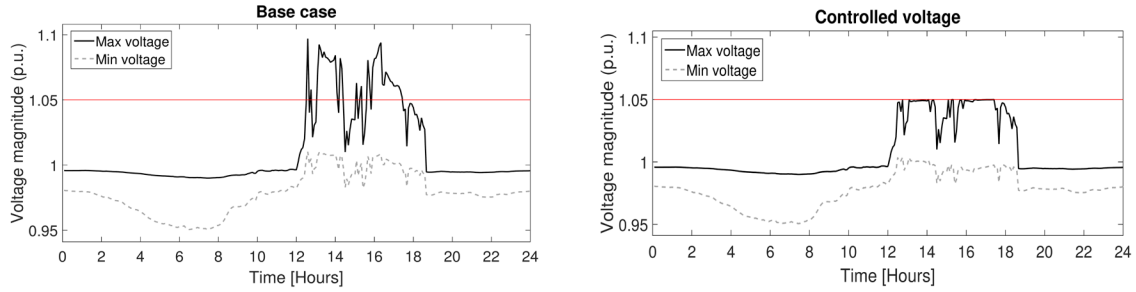

Figure 7 **left**) minimum and maximum network voltage profile for case 0 (no control), **right**) Minimum and maximum network voltage profile for case 1 (centralized control algorithm).

Whilst *Figure 7* present an aggregate view of the network voltages, *Figure 8* below shows the network node with the worst voltage profile, namely node 10 which exhibits the largest number of voltage (max) violations along the day. The black solid line in *Figure 8* shows the uncontrolled voltage of node 10 which exhibits over-voltages in the order of 10% in the middle of the day. Once the centralized control is activated (grey line), the voltage is successfully maintained below 1.05p.u. It is also worth noting that both the distributed and centralized algorithms are successfully controlling the PV power production to ensure a voltage within acceptable limits and that the two solutions are very close.
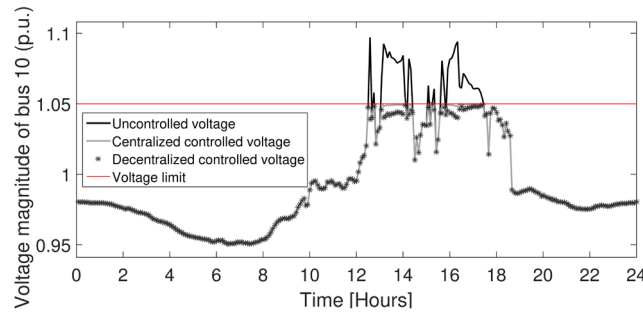

Figure 8 Voltage profile of node 10 without control (black solid line), after centralized control is activated (gray line) and when the distributed control algorithm is implemented (marker).

For the sake of completeness, *Figure 9* shows the curtailment of the power production of the 4 PV plants corresponding to the improvement in the voltage profile shown above.
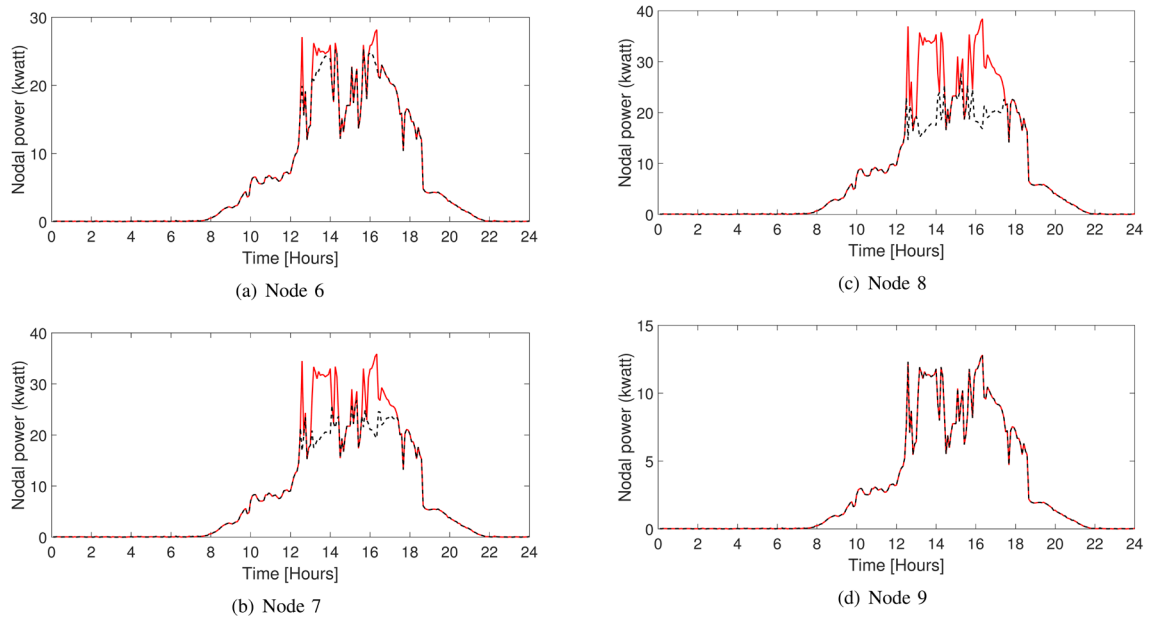
(a) Node 6

(c) Node 8

(b) Node 7

(d) Node 9

Figure 9 PV power production profile before (red solid line) and after control (black dashed line)

Figure 10 - left shows the minimum and maximum absolute difference in the voltage profiles obtained when solving the problem in a centralized and in a distributed way. It is worth observing that the maximum difference is in the order of 9×10^{-3}.

Next, the performances of both algorithms with respect to computational time and number of iterations is evaluated. Figure 10 - right shows the number of iterations required along the day so that the distributed version of the algorithm converges. As expected, the number of iterations is increased in the middle of the day, during the peak PV production period, during which over-voltages occur. However, it is worth noting that the amount of iterations reported in Figure 10 - right is compatible with the time requirements of a primary control algorithm. *Table 1* shows the mean CPU time for the solution of the centralized algorithm for the whole 24hr period when running the 24hr simulation 1000 times.[6] Even in this case, the amount of time required by the control algorithm justifies its adoption for voltage control.[7]

Table 1 CPU TIME REQUIRED BY THE CENTRALIZED ALGORITHM FOR THE 24HR CONTROL PERIOD

Number of simulations	Mean CPU time	Standard Deviation
1000	77.8 ms	12.2 ms

---

[6] The mean and standard deviation of the CPU time have been computed using an Intel i7-2720QM CPU, 2.2GHz.

[7] It is worth observing that the time required by solar plant power electronics to actuate a given power setpoint is negligible with respect to the computation times of Table 1. Indeed, nowadays PV power converters can implement changes in the power set-poitns below 10 ms.
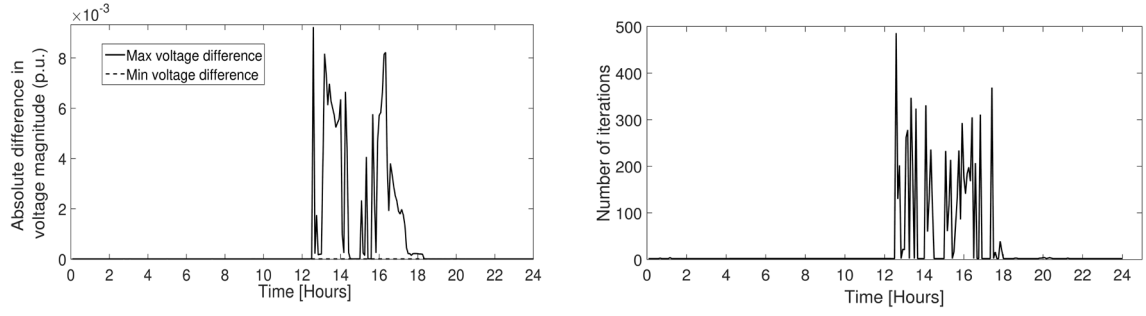
Figure 10 **left**) minimum and maximum absolute difference in voltage magnitude between the centralized and the distributed control algorithms, **right**) number of iterations for the distributed control algorithm.

Finally, we investigate the effect of the objective function on the results of the optimal control problem. To do so, we replace the logarithmic objective that guarantees a proportional fair scheduling of the PV plants, i.e., $U_g(P_g) = log(P_g + \Delta P_g)$, with a linear increasing function of their active power production, i.e., $U_g(P_g) = P_g + \Delta P_g$. The results of the simulation are shown in *Figure 11*, where we plot the 24hr scheduling of the smallest (*Figure 11* (a)) and largest (*Figure 11* (b)) PV plant for the two cases. It is worth noting that, on one hand, the smallest PV unit (node 9) is not curtailed under proportionally fair scheduling, whereas it is significantly curtailed in the case of the linear objective function. On the other hand, the largest PV unit connected at node 8, is curtailed more under the proportional fair scheduling and less when a linear objective is used.
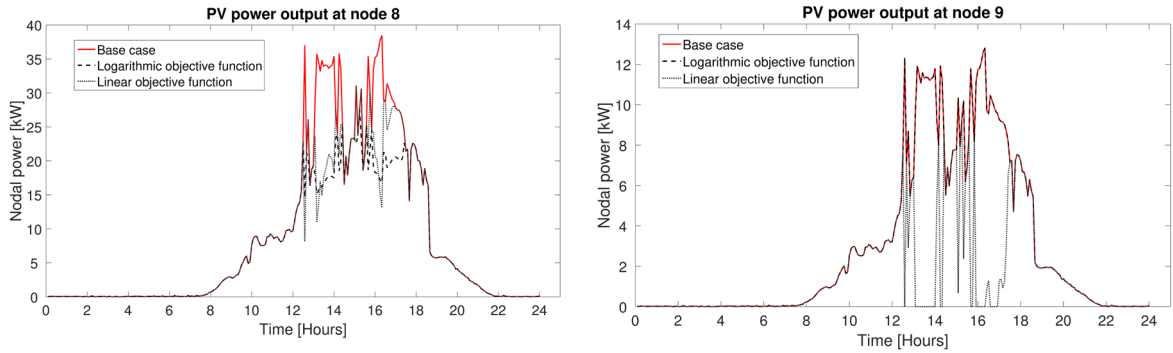

Figure 11 **left**) PV power production profile at node 8 (i) before control (red solid line), (ii) control with logarithmic objective (black dashed line), (iii) control with linear objective (black dotted line). **right**) PV power production profile at node 9 (i) before control (red solid line), (ii) control with logarithmic objective (black dashed line), (iii) control with linear objective (black dotted line).

3.2.4 Conclusions and Outcomes

In this study, we have investigated the potential of distributed PV plants for providing voltage control to low voltage grids. The optimal control problem is formulated in such a way that it guarantees a proportionally fair scheduling of the controllable PV units. Starting from the centralized formulation of the optimal control problem, a distributed algorithm for handling over-voltages was also designed. The distributed version of the algorithm relies on a dual de-composition framework and has been shown to converge to the same solution as the centralized algorithm. Even if the numerical analysis has shown that the distributed version of the algorithm requires a relatively large number of exchanged messages to converge, it does represent a useful solution when the state estimation output is asynchronous with respect to the controller actions. Indeed, in this case the controller obtains iterative refinements of the sensitivity coefficients. The performance of the control algorithms has been evaluated using the CIGRE LV benchmark grid. Both algorithms have successfully reduced over-voltages and maintained the

network voltage profile within safe limits. Finally, the computational time of the centralized algorithm, as well as the number of iterations of the distributed version, justify their adoption as primary voltage controllers.

This study is also resulted in the publication of the below research conference paper [8].

Numa Gueissaz, Konstantina Christakou, Jean-Yves Le Boudec, and Mario Paolone, "Fair Control of Distributed PV Plants in Low Voltage Grids", 2017 IEEE Innovative Smart Grid Technology Conference Europe, Turin, Italy.

3.3 Utilization of different media communications

The objective of this sub-section is to use different communication gateways (GSM / PLC / RF) developed in the CTI project (see Figure 12) and test them in the Relne laboratory. The issue is that having an industrial prototype is very complicated and economically unsustainable. Thus, it is decided to use the available and well tested commercial solutions.
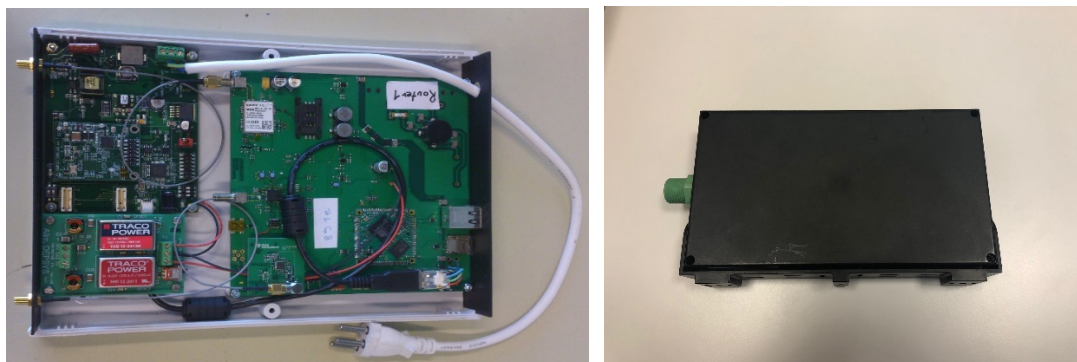
Figure 12 The developed board to use different communication gateways in the CTI project vs industrial product

The GSM has been used as the primary communication way of GridEye in majority of DEPsys projects. The Broadband Power Line communication is tested for the network monitoring and the estimation of sensitivity coefficients, as shown in Figure 13. The WiMax technology is tested for the network monitoring, the estimation of sensitivity coefficients, and the decentralized and model-less control as shown in Figure 14

100 to 101: 54.5 Mbits/sec
100 to 102: 28.3 Mbits/sec
104 to 102: 15.7 Mbits/sec

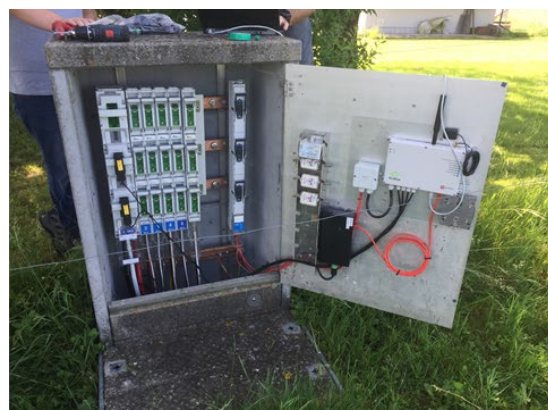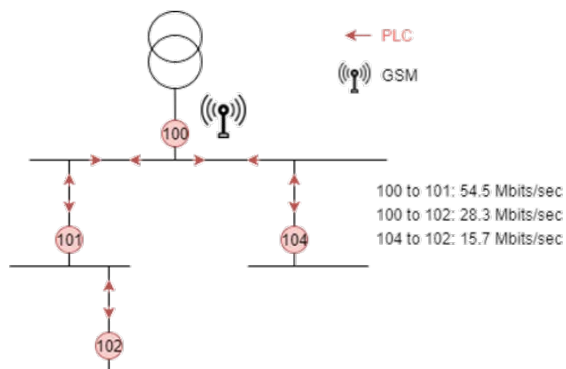Figure 13 Using Broadband Power Line communication.
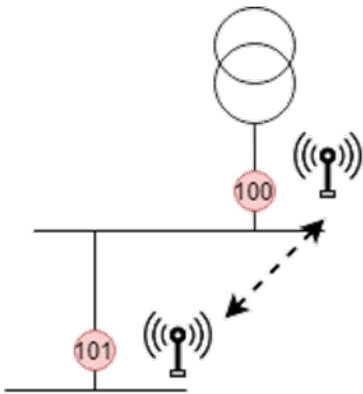
Figure 14 Using WiMax communication.

3.3.1 Conclusion

All three different communication medias were successfully tested and the results are similar in term of performances. Technically speaking, all three communication media are fully transparent for the GridEye devices as all of them are based on the TCI/IP protocol. However in majority of cases, the Cellular communication enables easier plug and play integration and is cost effective compared to the two others communication possibilities (PLC and WiMax). The choice of the integration of the cellular communication directly into the GridEye device was an appropriate approach. The other technologies can be also used in backup or in case of a low cellular network coverage.

4 Cyber security protection strategy

4.1 Introduction

We recall the tasks to be carried out defined within the framework of this project:

- **Threat analysis** - development of a computer threat model for a dynamic low-voltage network with sensors and loads.

- **Risk management** - prioritizing threats to potential impacts in order to design effective countermeasures to provide a certain level of trust at a reasonable cost.

- **Design of the system security architecture** - proposal of security architecture for the low-voltage network management system taking into account the security requirements established on the basis of threat analysis as well as functional requirements.

- **Implementation of protection mechanisms** - based on the security architecture implementation of protection measures.

- **Security tests** - intrusion tests simulating hostile activities of a potential attacker on a secure system deployed in the REINE laboratory.

We will now summarize these and additional tasks that were performed in the context of this project.

4.2 Threat modeling and risk assessment

First of all, the architecture of the low voltage system (e.g. GridEye) was analyzed. This system is a modular solution consisting of sensors and intelligent elements distributed in the field (low-voltage networks) with a centralized backend system.
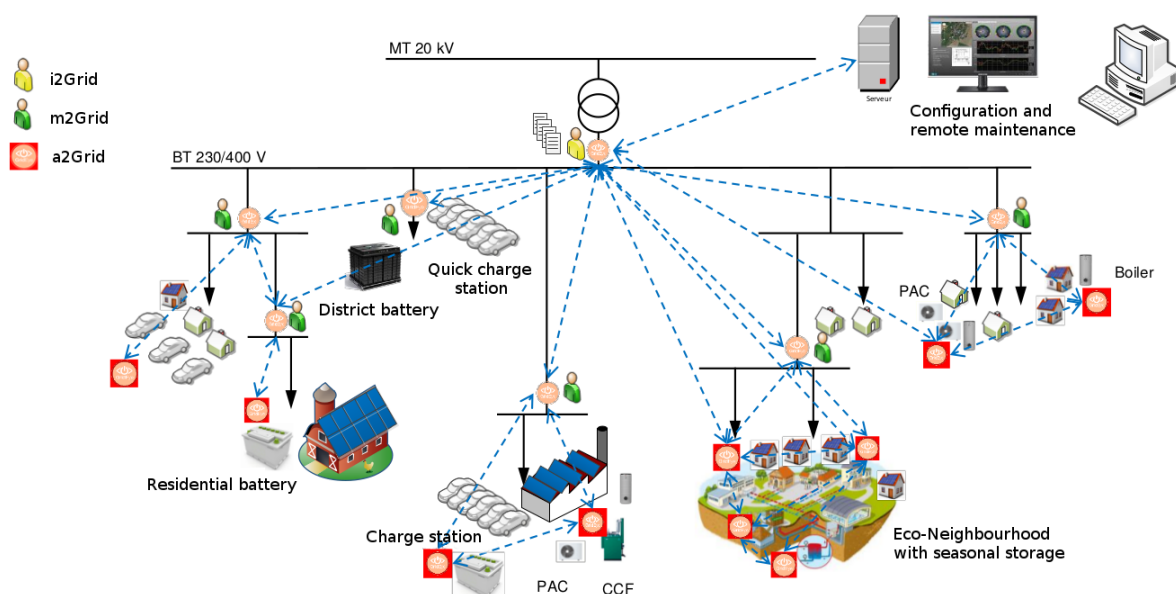

Figure 15: High-level Architecture of GridEye system

In the field, the modules mainly fulfil three different roles. The i2Grid functionality is a gateway to the centralized infrastructure through which the information collected by the sensors as well as the action orders sent by the central server pass. The m2Grid functionality is a sensor that collects different values from the low voltage electrical grid at a specific location. Finally, nodes with the a2Grid functionality allow actions to be performed on the network (load engagement) that it receives via the i2Grid gateway (see Figure 15). At the beginning of the project there were three distinct types of GridEye modules, but towards the second half of the project only one type of module remained regrouping these three functionalities.

The GridEye system modules are built on a hardware platform based on a specific System-on-Chip (SoC). The analysis therefore focused on this hardware base as well as on the aspects of communication between the modules and the backend server.

Taking the elements of the system architecture analysis as a basis, a complete threat analysis was performed. Threat analysis provides an overview of the system from a security perspective and its weaknesses. The key point of a threat analysis is a DFD (Data Flow Diagram) as well as an in-depth analysis using the STRIDE framework (Spoofing, Tampering, Repudiation, Information Disclosure, Denial of Service). Figure 16 shows one of the DFDs of the GridEye system.

In general, it is not realistic to face all the threats in terms of resources (time and money) required. In view of the threats discovered, a risk analysis was carried out to prioritize the remediation to be performed in order to optimize the resources required for IT risk management. Based on the criticality of the impact and the probability of each threat, a list of risks has been established, from the most critical to the least significant.
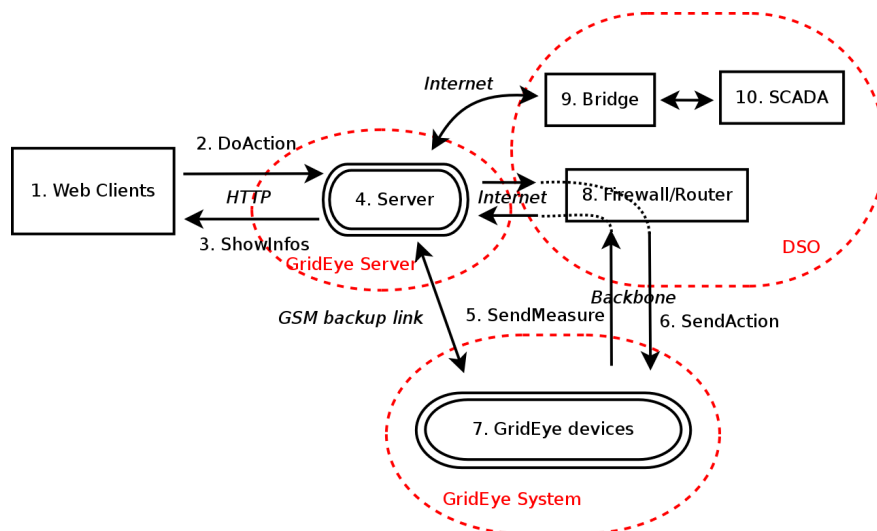
Figure 16: GridEye DFD (Data-Flow Diagram)

A risk is the probability that a given vulnerability will be exploited by a threat leading to an impact (technical and business) on the target system. More specifically, in the current system, probability is directly related to the difficulty of executing a certain specific attack. The proposed scale uses only three different levels: high, medium and low. Figure 17 graphically presents the identified risks. For confidentiality purposes the exact details of the identified risks are not disclosed in the current report.

Figure 17: Graphical representation of identified cyber risks

4.3 Identified risks and remediations

We can see that some risks have a high probability with a high impact. These are the risks that were addressed in the first place. The ove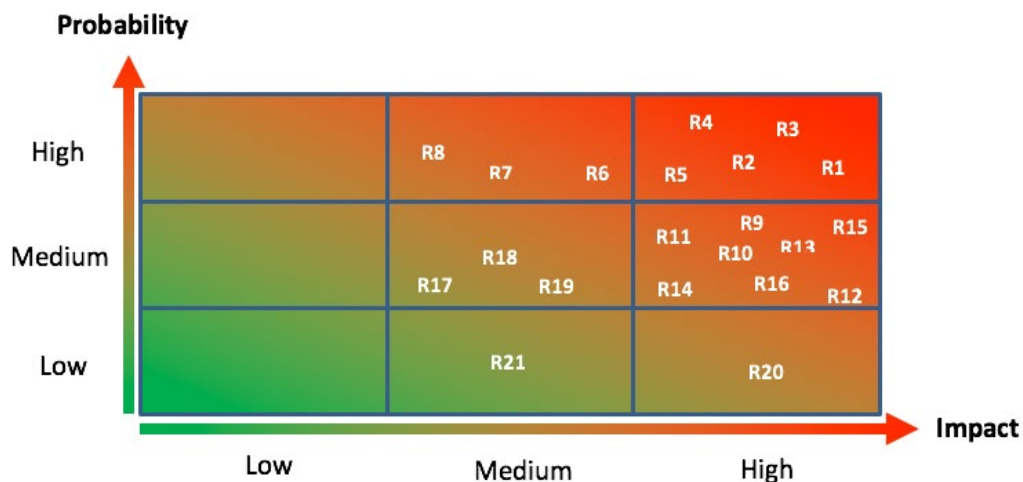rall remediation strategy consisted in proposing countermeasures and protection mechanisms to reduce the probability of a cyberattack. These mechanisms are described in the Security Requirements documents as well as architectural documents. These specifications were then used to implement the protection mechanisms in the GridEye system but also in other possible projects (e.g. Internet of Things). The effort required to implement the countermeasures was estimated in order to optimize the resources available. It should also be noted that since the GridEye system is in its active development phase, the functional requirements, architecture, communication protocols and other technical aspects are not yet fully defined. These points were considered in the planning of the remediation strategy.
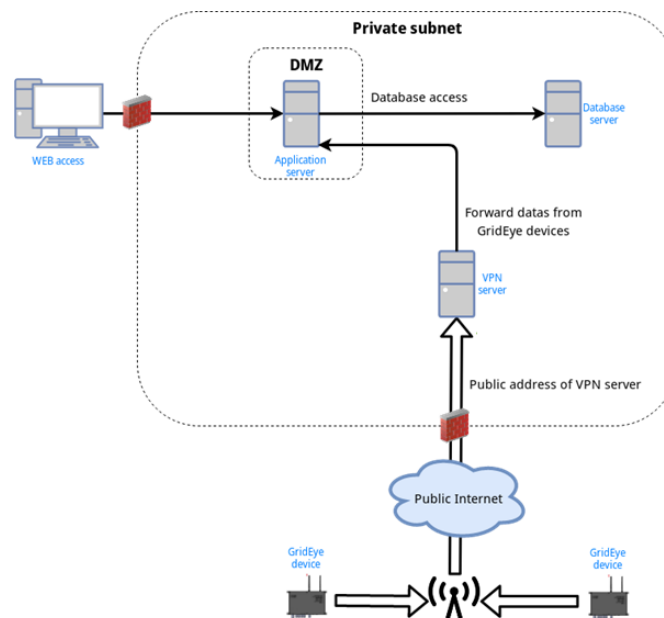

Figure 18: Functional security architecture for a Smart Grid GridEye network

Figure 18 shows an overview of the proposed security architecture for GridEye network. The purpose of this architecture is to isolate the critical infrastructure of the GridEye system from the public network (e.g. Internet) and at the same time to provide flexibility and ease of use for the management and monitoring functions of the GridEye modules. The architecture mainly addresses the risks R4 and R16, as well as partially R11 and R13.

The GridEye modules are on a local network managed by DEPsys. Connectivity between modules and back-end servers is provided by a Virtual Private Network (VPN). The connection to the VPN server is made by means of a private APN within the public GSM network or the DSO's optical fiber. The only requirement is that the VPN server port is accessible from the internal network on which the GridEye modules reside.

Tests were carried out on several VPN solutions in terms of connectivity in terms of signal quality, performance, bandwidth available in the channel and CPU/memory load on the module side deployed in the field.

ID	Sleep	Nb of packets	Size	Nb of clients	CPU Usage	
					OpenVPN	GridEye VPN
T00	1	60	10Ko	50	<5%	<5%
T01	1	60	10Ko	100	<5%	<5%
T02	1	60	10Ko	150	<5%	<5%
T03	1	60	100Ko	50	<10%	<10%
T04	1	60	100Ko	100	<10%	<10%
T05	1	60	100Ko	150	<15%	10-20%
T06	1	60	1Mo	50	45-60%	30-40%
T07	1	60	1Mo	100	50-70%	40-50%
T08	1	60	1Mo	150	50-75%	40-50%
T09	5	60	10Ko	50	<2%	<2%
T10	5	60	10Ko	100	<3%	<2%
T11	5	60	10Ko	150	<3%	<2%
T12	5	60	100Ko	50	<8%	<5%
T13	5	60	100Ko	100	<8%	<6%
T14	5	60	100Ko	150	<10%	<6%
T15	5	60	1Mo	50	15-20%	10-15%
T16	5	60	1Mo	100	25-40%	15-30%
T17	5	60	1Mo	150	40-55%	30-40%

Figure 19: Usage of server resources based on the number of connected clients and exchanged traffic

For the example in Figure 19, the use of VPN server resources is shown according to the number of connected clients. Following the tests, the VPN solution was adapted by integrating it within GridEye modules in an embedded environment. Currently the VPN-based security system is successfully used in production for GridEye modules and can be easily adapted to other SmartGrid scenarios as well as use in the field of Internet-of-Things (IoT).

4.4 Log Management

In this section, we summarize the different tasks completed or being carried out since the beginning of the project concerning the management of logging information (logs) in order to remedy the different risks (R5, R7, R8 and R20).

First of all, each of the risks has been studied. For risks that can be (partially or fully) remedied through the use of logs, the solution has been studied in detail for both the server side and the GridEye systems.

This study contains the list of information that must be sent in the logs (e. g. the GridEye ID, application name and file that generated the log), their format and the types of logs to be sent at what time in order to be able to, for example, link the different GridEye systems that have a common problem.

The log architecture currently in place was also analyzed in order to choose an ideal solution that would easily centralize the type of logs required and separate the logs between the different applications.
We then looked for solutions to solve the problems identified during the previous analysis and it became clear that it was necessary to find a solution to gather and centralize the logs (user, system, application, etc...) of all connected devices at a single point so that they could then be processed, managed and visualized in order to intervene as quickly as possible.

There are several solutions on the market (open or private) to centralize remote system logs. The different systems have been sorted according to the following points:

- Prices
- Efficiency and effectiveness
- CPU consumption
- RAM consumption

The last two points being the most important because we are in the world of embedded systems that have limited resources.

According to the previous criteria, the rsyslog program was chosen to centralize the logs. Rsyslog is a free software, of client<->server type, used on Unix operating systems. It transfers event log messages (basic logs on the platform or customized) from the "client rsyslog" to an "rsyslog server".

Rsyslog has been tested:

- In borderline cases (many logs to be reported or very few)
- In ideal cases or in accordance with reality

The result was that Rsyslog is perfectly suited for this application.

Once the logs were centralized, a centralized solution was also needed to visualize and manage them in a simple way. For this part too there are several solutions on the market. The following points were analyzed to select the system:

- Features (email alert system)
- Prices
- Possibility of modification (open source, API,...)

A log management system, Elasticsearch, emerged from the analyses. This system has been tested in more detail to see how it works from log collection to log visualization to log identification and grouping by GridEye, per hour or any other information we have in the logs.

4.5 Cybersecurity intrusion tests

After performing abovementioned activities and according to the initial planning, a penetration test was performed on the GridEye infrastructure. For confidentiality purposes, we will only disclose some elements of the report and general structure of the security tests.

These tests followed best practice in terms of penetration testing for infrastructure and embedded systems. It has to be noted that a person which was not familiar with the details of the project nor with the security architecture of the GridEye system performed the below-mentioned steps. Following phases were executed against DEPsys GridEye system:

- **Information gathering** - When trying to gather information about a company and their products, analysing their website is often a good starting point. By analysing it, we will try to find information about the kind of technology they use or any information about the employees to maybe start a phishing attack in order to retrieve credentials or any other useful information.

- **Black box testing** - During this phase of the testing, no complementary information was provided by DEPsys besides the IP address of the application server. Black box tests and deduced observations were conducted on the test environment provided by DEPsys.

- **Authenticated testing** - For this part of the vulnerability assessment, an account without elevated privileges was created by DEPsys and used to attempt a privilege escalation or any kind of exploitation available.

Nothing critical was found during the black box stage of the analysis. Some low-risk cases were revealed and reported. During the authenticated user analysis, a few flaws were found but nothing that would directly compromise the device or the infrastructure. This also follows from the risk analysis performed at the beginning of the project. Even though some of the most critical risks were mitigated through the design and deployment of a new security architecture, the mitigation of the scenario where an attacker has a direct access to the GridEye module was undertaken towards the cybersecurity protection strategy activity of the project.

4.6 Conclusion

The goal of the Cybersecurity protection activity of the present project was aimed at proposing some generic mechanisms for protection of Smart Grid networks. The example of DEPsys GridEye system was taken. During this activity a full threat model of the system was established, a risk analysis performed and a security architecture developed. The security architecture is based on a Virtual Private Network (VPN) which provides confidentiality and integrity of information exchanged between Smart Grid devices and back-end infrastructure (back-end servers). This security architecture has been successfully tested and deployed in production. A penetration test has been performed on the back-end infrastructure (including web-based frontend), on the infrastructure connecting modules as well as on the modules themselves. The result show that most critical risks identified at the beginning of the project were mitigate and the next step is to secure the module itself from the hardware security perspective.

5 Validation Tests

In this section, first we present the validation tests performed in the Reine laboratory with respect to deployment of GridEye devices. The test case is described in section 5.1. Simulation results of the test case based on power flow algorithms as well as model-aware algorithms for computation of sensitivity coefficients are presented in section 5.2. In section 5.3, we described Data Acquisition System of Reine laboratory (DASRIL) used for validation tests. Then, the real test results in the Reine laboratory including measurements obtained from both DASRIL and GridEye devices installed in the laboratory are presented and analysed in section 5.4. Finally, we present validation test results for a real grid control algorithm application using GridEye devices in a real distribution grid in Switzerland in section 5.5.

5.1 Test case description

In this section, we describe the validation test case in the Reine laboratory. The objectives of this test case is to validate deployment of GridEye devices and developed algorithms for computation of voltage sensitivity coefficients in the known laboratory environment, under a realistic distribution grid operation scenario. In this respect, distribution grid of the Reine laboratory and its connected installations are configured to present an inductive low voltage grid including photovoltaic (PV) power production during 6 hours in the middle of a summer day.

The grid composed of 4 buses connected via 3 lines. A transformer and a 110m cable connects this grid to the public electrical grid of HEIG-VD campus at Chesaux, Yverdons-les-Bains, Switzerland. Grid configuration as well as installation connected to the grid are shown in Figure 20. Table 2 presents nodal (bus) data corresponds to this grid test case. Bus 0 is a slack bus that will be used in power flow analysis in following sections. Line and transformer data are presented in Table 3. Note that Line 1 models the transformer and the connecting 110m cable in series. The line and transformer parameters are presented in per unit values where the base power value (Sbase) is 1 kW and the base voltage value (V LN base) is 230 V. It is worth noting that the parameters of line number 2, 3, and 4 are not representing a real LV grid due to very high X/R ratio.
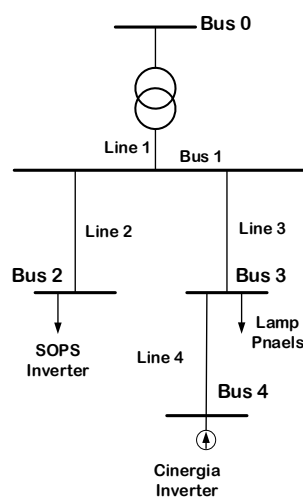

Figure 20 Grid Configuration in Reine laboratory

Bus Number	Bus Name (Reine)	Nominal voltage (RMS LN) [V]	Connected installation	Installation connection name (Reine)

Hes·so
Haute Ecole Spécialisée
de Suisse occidentale

0	-	230	-	-
1	N1	230	-	-
2	N3	230	SOPS Inverter	Resource 9
3	N6	230	Lamp Panels	Resource 7
4	N9	230	Cinergia Inverter	Resource 8

Table 2 Bus data of the grid in Relne laboratory

Line Number	Line name (Relne)	From bus	To bus	R (pu) Phase 1U	X (pu) Phase 1U	R (pu) Phase 2V	X (pu) Phase 2V	R (pu) Phase 3W	X (pu) Phase 3W	Current Limit per phase (Imax) [A]
1	-	1	0	1.23 e-3	5.81 e-4	1.23 e-3	5.08 e-4	1.23 e-3	5.08 e-4	33.35
2	L1+ L2	1	2	7.36 e-6	2.31 e-3	7.42 e-6	2.33 e-3	7.41 e-6	2.33 e-3	34.50
3	L5	1	3	3.67 e-6	1.15 e-3	3.71 e-6	1.16e-3	3.72e-6	1.17 e-3	34.50
4	L4+ L6+ L7	3	4	6.73 e-4	3.56 e-3	6.73 e-4	3.55 e-3	6.73 e-4	3.55 e-3	34.50

Table 3 Grid line data in Relne laboratory

Next, we describe the injection/absorption power profiles from connected installations during the test period. The SOP connected at bus 2 consume power according to per phase pre-set-points depicted in Figure 21. The set points are obtained by aggregating residential power consumption data connected to a low voltage grid in Chapelle, Switzerland. The Cinergia inverter injects power at bus 4 according to a PV production profile during a summer day in Chapelle, Switzerland, as depicted in Figure 21. The lamp panels present a piece-wise constant power consumption at bus 3 (step changes over each two hours) profile as shown in Figure 21. Note that positive values shows power injection (production) and negative values show power consumptions.
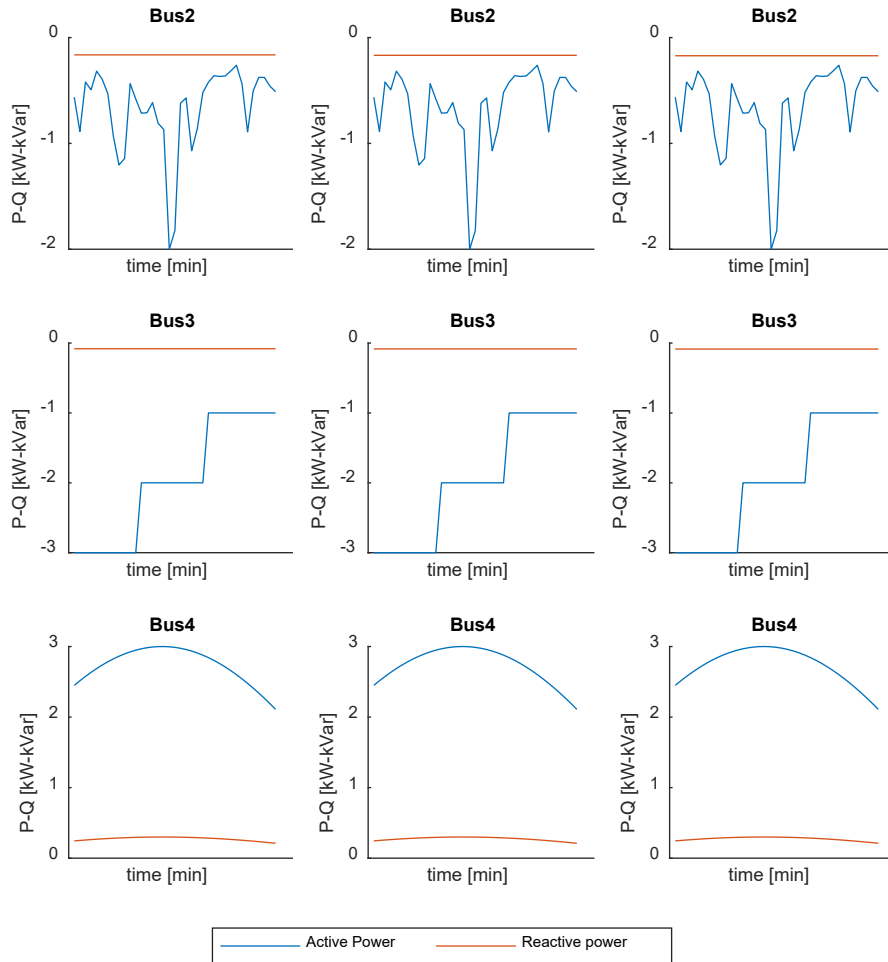
Figure 21 Power injection/absorption profiles with 10 minutes time steps during 6 hours

5.2 Pre-validation simulation

At pre-validation stage, we simulate the test case with power injection/absorption profiles according to Figure 21, to find the voltage levels as well as line power flows (operation points). In this respect, we performed a three-phase power flow simulation based on Newton-Raphson algorithm. Then, we analyzed the results (operation points) based on; a) direct computation (using inverse of Jacobian matrix), b) Analytical and model-aware method proposed in [6], and c) Gauss-Seidel computation as proposed in [9], to find the voltage sensitivity coefficients with respect to the real and reactive power injection. For the sake of brevity, we only present the results for phase 1 as the level of imbalances between the phases is very low. Figure 22 shows the results in which Kvp (i,j) denotes sensitivity of voltage at bus i with respect to power injection at bus j. Similarly, Figure 23 shows the results in which Kvq (i,j) denotes sensitivity of voltage at bus i with respect to power injection at bus j. Note that, the results of direct computation are the reference values according to the definition of the sensitivity coefficients.
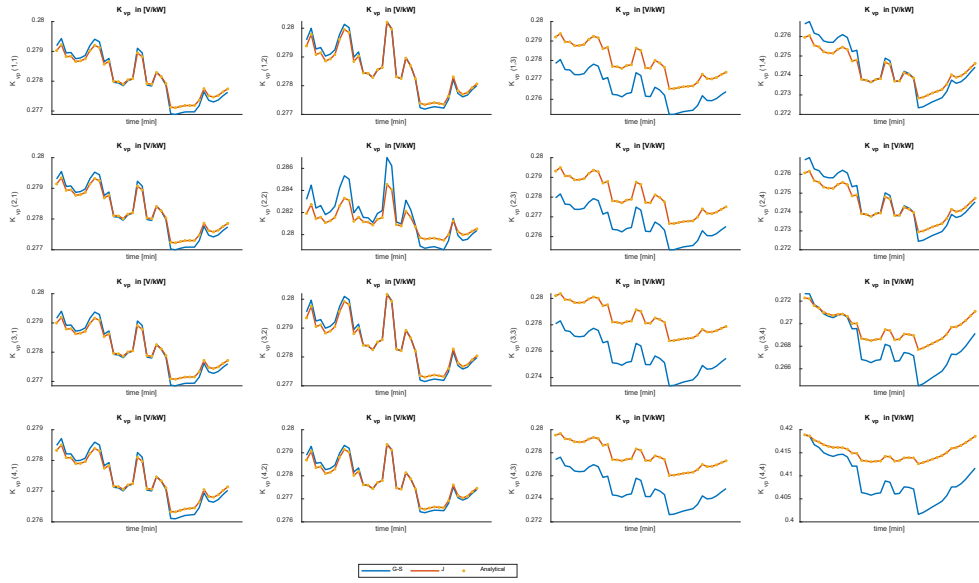
Figure 22 Sensitivity coefficient of voltage with respect to active power injection at phase 1. Red: Jacobian computation, Yellow stars: Analytical method proposed in [6], Blue: Gauss-Seidel method proposed in [9]
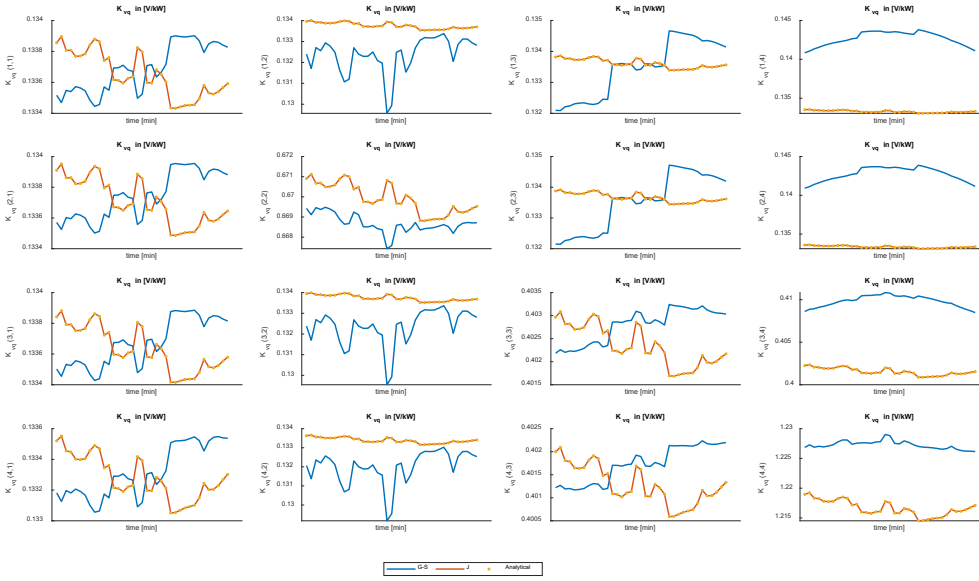

Figure 23 Sensitivity coefficient of voltage with respect to reactive power injection at phase 1. Red: Jacobian computation, Yellow stars: Analytical method proposed in [6], Blue: Gauss-Seidel method proposed in [9]

The mean value of sensitivity coefficients computed based on inverse of Jacobian matrix (reference values) are presented in Table 4.

Kvp(i,j) - Reference	i = 1	i = 2	i = 3	i = 4

	i = 1	i = 2	i = 3	i = 4
j = 1	0.2722	0.2725	0.2719	0.2686
j = 2	0.2723	0.2751	0.2720	0.2687
j = 3	0.2721	0.2725	0.2725	0.2643
j = 4	0.2714	0.2718	0.2718	0.4070
Kvq(i,j) - Reference	**i = 1**	**i = 2**	**i = 3**	**i = 4**
j = 1	0.1308	0.1309	0.1307	0.1304
j = 2	0.1308	0.6556	0.1308	0.1305
j = 3	0.1307	0.1308	0.3937	0.3930
j = 4	0.1304	0.1305	0.3927	1.1909

Table 4 Mean values of voltage sensitivity coefficients at bus i with respect to active power injection at bus j

The results of the analytical method proposed in [6], are in good agreement with the reference values. Finally, the relative differences between the sensitivity coefficients computed based on the Gauss-Seidel method and the reference values are presented in Figure 24. We can see that the relative differences for computation of Kvp is below 1%, whereas the relative difference of Kvq is below 7%.
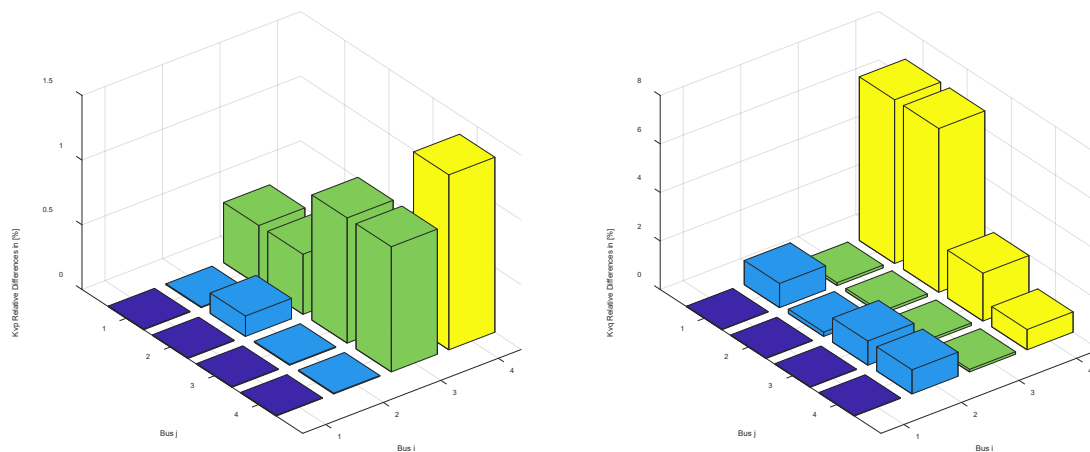

Figure 24 Relative differences between the sensitivity coefficients computed based on the Gauss-Seidel method and the reference values in [%].

5.3 Data Acquisition System of ReIne Laboratory (DASRIL)

Data Acquisition System of ReIne Laboratory (DASRIL) is made up of both National Instrument and LEM products. Experimental setup for SMILE-FA tests is resumed in Figure 25.
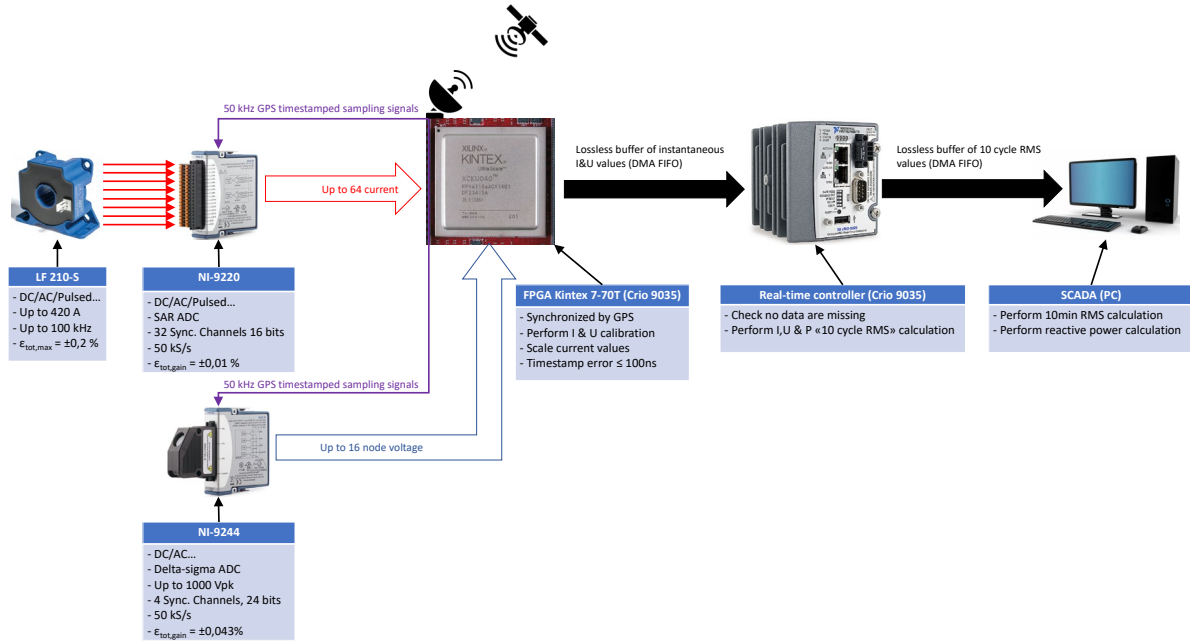

Figure 25 Data Acquisition System of ReIne Laboratory

Currents are acquired through LF 210-S current sensors [10], resistor transducer (not represented) and NI-9220 analog-to-digital converter cards [11]. LF 210-S is a closed loop compensated current transducer able to gather AC, DC or pulsed current up to 420A (200A in nominal condition). Bandwidth at -3 dB is 100 kHz, whereas maximal total error at nominal current reach ±0.2%. The NI-9220 is composed of 16 synchronous channels with a maximal sampling rate of 50 kS/s. Typical gain error for a calibrated card is about 0.01% of reading. The current in the neutral wire is not measured but deduced by the three-phase currents.

NI-9244 acquired and digitized node voltages up to 1000 Vpk. The NI-9244 include 4 synchronous channels (3x phase-neutral and 1x neutral-earth) with a maximal sampling rate of 50 kS/s. Typical gain error for a calibrated card is about 0.043% of reading. Finally, the NI-9244 include an internal master time to synchronize both NI-9220 and NI-9244, typical time synchronization error is about 78 ns.

Each sample acquired by NI-9220 and NI-9244 cards are send to the FPGA of a CompactRIO 9035 system. FPGA clock is synchronized with a GPS system through NI-9467 card [12]. Synchronization of FPGA with a GPS allow an accurate timestamping for each sample, expected jitter is lower than 100 ns.

Data from FPGA are send to a real-time controller trough a very high speed and lossless buffer called Direct Memory Access channel. Real-time controller check if some data are missing and evaluate 10-cycle RMS values. 10-cycle RMS values are calculated according to the following process:

For currents and voltages, 10'000 samples are recorded, RMS values are calculated according to the (14):

$$x_{10-cycle,rms} = \sqrt{\frac{1}{n}\left(\sum_{0}^{n=10000} x_n^2\right)} \tag{14}$$

This method is not compliant with 61000-4-30. However, for 50 Hz power grid, the error done on RMS value should be less than 1%.

For real power, instantaneous values of current and voltage are multiplied and aggregated over 10000 samples, then the real power is calculated according to the (15):

$$P_a = \frac{1}{n}\sum_{0}^{n=10000} u \times i \tag{15}$$

As mentioned in IEC 61000-4-30, 10-cycle RMS values are timestamped at the timestamp of the 10000 sample.

10-cycle RMS values are send each 200 ms to a host computer for supervising, storing and evaluating both 10 min RMS values and real power (10-cycle and 10 min RMS values). 10 min RMS values are calculated according to the process describe in 61000-4-30 for S-class device. Real power is assessed according to power triangle formulas.

$$\left|S_{10-cycle,RMS}\right| = I_{10-cycle,RMS} \times U_{10-cycle,RMS} \tag{16}$$

$$\left|Q_{10-cycle,RMS}\right| = \sqrt{S_{10-cycle,RMS}^2 - P_{10-cycle,RMS}^2} \tag{17}$$

5.4 Validation tests in ReIne

In this section, we present the results of validation tests in the ReIne laboratory environment. In this respect, first we compare the results of power flow simulations (voltages at all buses and power flows on all lines) with the measurements acquired by Data Acquisition System of ReIne Laboratory (DASRIL). Figure 26 shows the voltage comparisons regarding average values computed over 10-minites time steps during 6 hours of the test for three phases. The average relative differences between the measured voltages and voltage computation based on power flow simulation are below 0.05% as depicted in Figure 27.
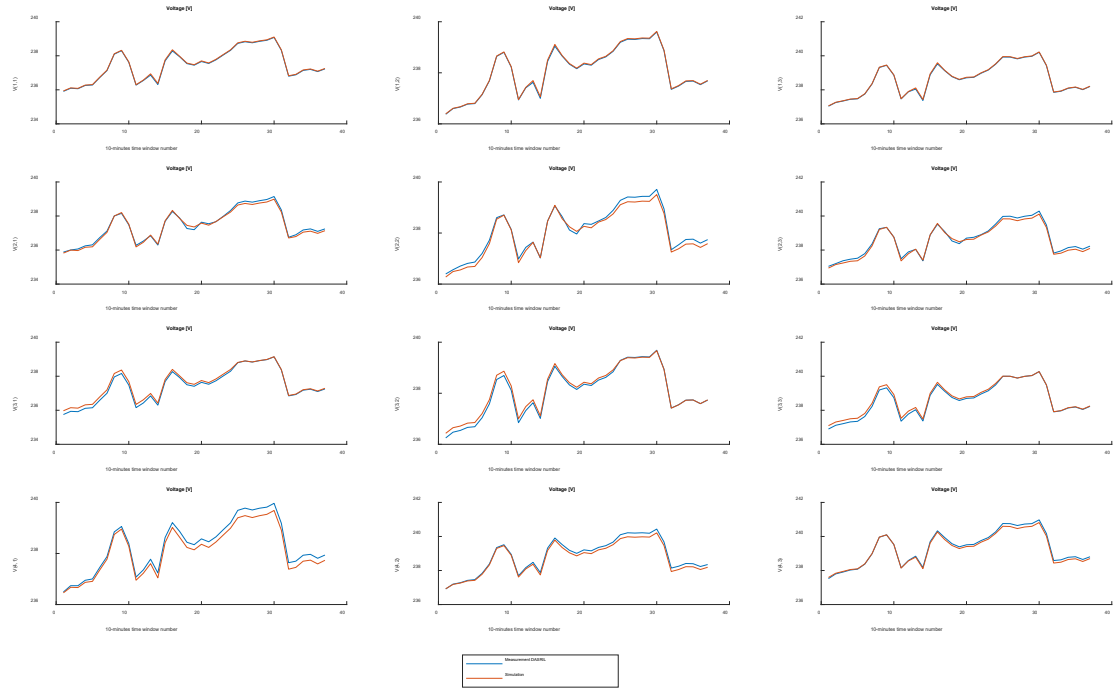
Figure 26 DASRIL voltage measurements vs power flow simulation results. V(b,φ): voltage at bus b, phase φ.
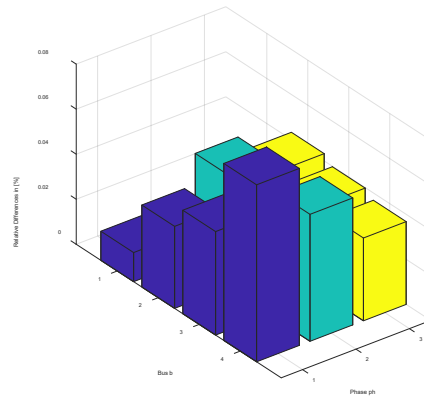

Figure 27 relative differences between the measured voltages and voltage computation based on power flow simulation in [%]

Figure 28 shows the power flow comparisons regarding average values computed over 10-minutes time steps during 6 hours of the test for three phases. The average relative differences between the measured powers and power flow computation based on power flow simulation are below 8% as depicted in Figure 29. Here the error of power measurements for lines 1 and 3 might be originated by error of calibration of line current sensors.
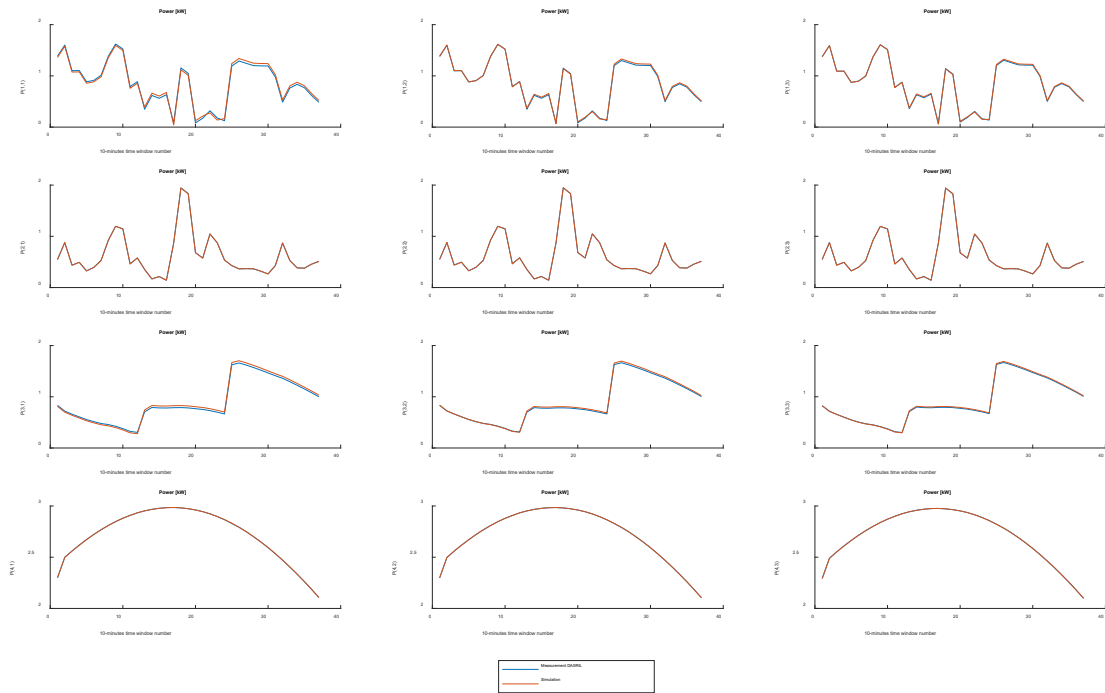
Figure 28 DASRIL line power flow measurements vs power flow simulation results. P(l,φ): power flow on line l (at from bus according to Table 3), phase φ.
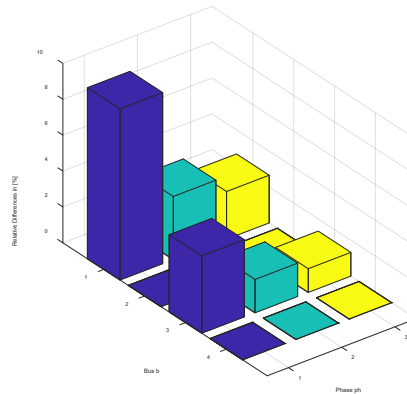

Figure 29 relative differences between the measured line power and power computation based on power flow simulation in [%]

Finally, in Figure 30 we present a comparison between the voltage sensitivity coefficients with respect to real power injections resulted from:

a) Direct computation based on inverse of Jacobian matrix – reference values (Jacobian),

b) Analytical and model-aware method proposed in [6]

c) Model-less method

As we can see in this figure, the model-less results are in good agreement with the reference values. The relative difference between the average values of model-less sensitivity coefficients and the

reference values are below 6% as shown in Figure 31. Note that in this case, the sensitivity coefficients of Model-less method are calculated using a limited number of measurement data.
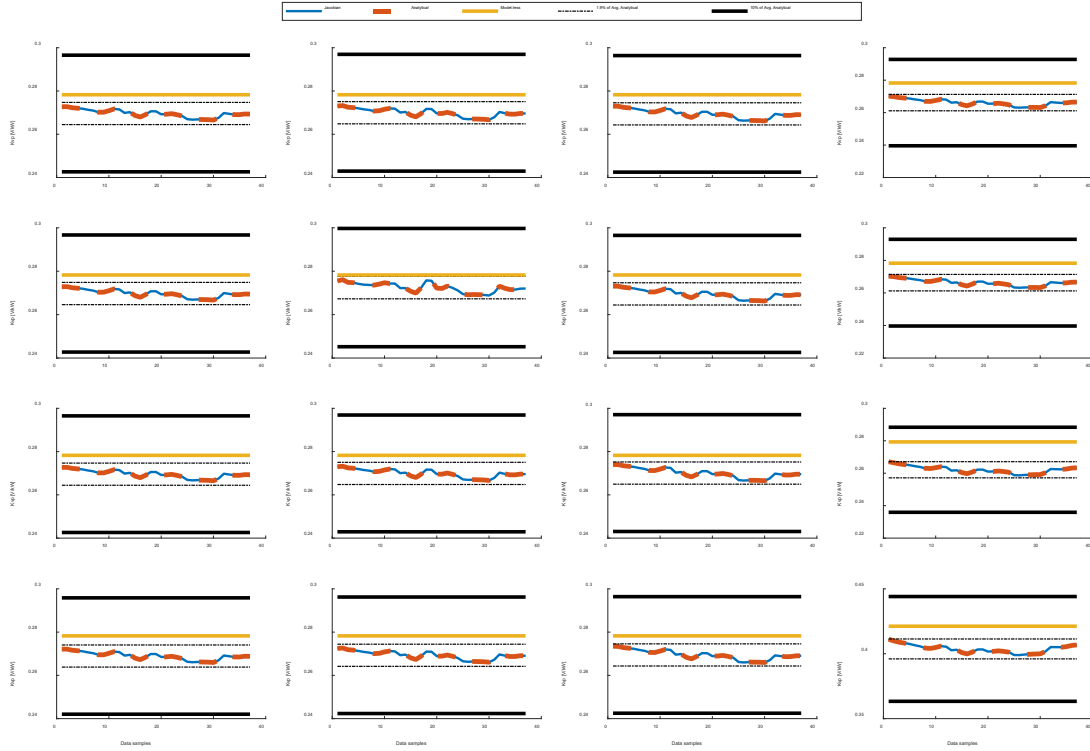

Figure 30 Sensitivity coefficient of voltage with respect to active power injection at phase 1. Blue: direct computation based on inverse of Jacobian matrix. Analytical: Analytical method proposed in [6]. Model-less: Model-less method
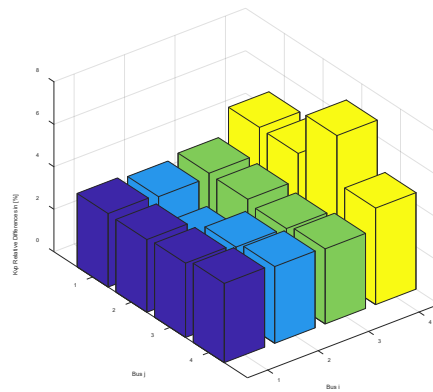

Figure 31 Relative differences between the sensitivity coefficients computed based on the model-less method and the reference values in [%]

5.5 Network control in real field

A model-less and decentralized optimal control approach is developed by DEPsys based on the estimated sensitivity coefficients. The developed method is implemented and successfully tested in a distribution network in Switzerland. Figure 32-left shows the single line diagram of the network, PV installation of 200 kWp on node 2 (N2), the local communication between GridEye modules as well as the communication between GridEye modules and GridEye server and between GridEye server and DSO servers. The PV inverters and the GridEye installation at node 2 are shown in Figure 32-right. It should be noted that in node 2, the same GridEye device that is used for the measurement and monitoring is also used for the control of the PV inverters.

In this case, the PV installation has caused the risk of overvoltage within the network. The DSO needs to ensure that voltages remain within the acceptable levels while the production of the PV installations are maximized. Here, the reactive power capability of the inverters are initially used for the voltage control and then if it is needed the active power curtailment is considered. Figure 33 shows the 3-phase voltage profiles at node 2 as well as the PV inverters active and reactive power outputs for the case without control (top) and the case using the GridEye optimal control (bottom). The results demonstrate that the developed model-less and optimal control approach can effectively control the voltages at the desired value (here 245 V) while the production from the PV installations are maximized.

It should be noted that GridEye system provides a wide range of application for visualization, control, and digitalization of distribution grids. Only using the optimal control application, the return of investment for 2 GridEye modules is achieved in 2-years.
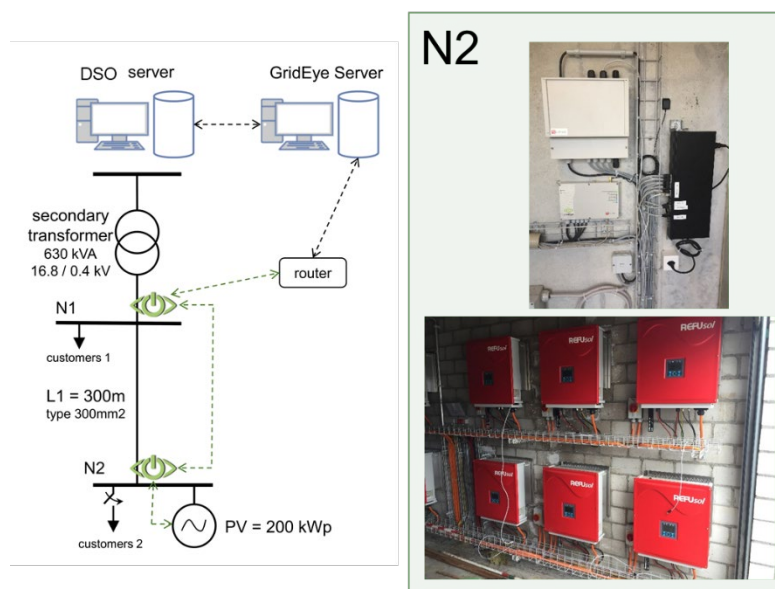

Figure 32 Application of the sensitivity coefficients and GridEye for the optimal grid control. left) single line diagram of network and communication structure, right) GridEye installation and PV inverters at node 2 (N2).
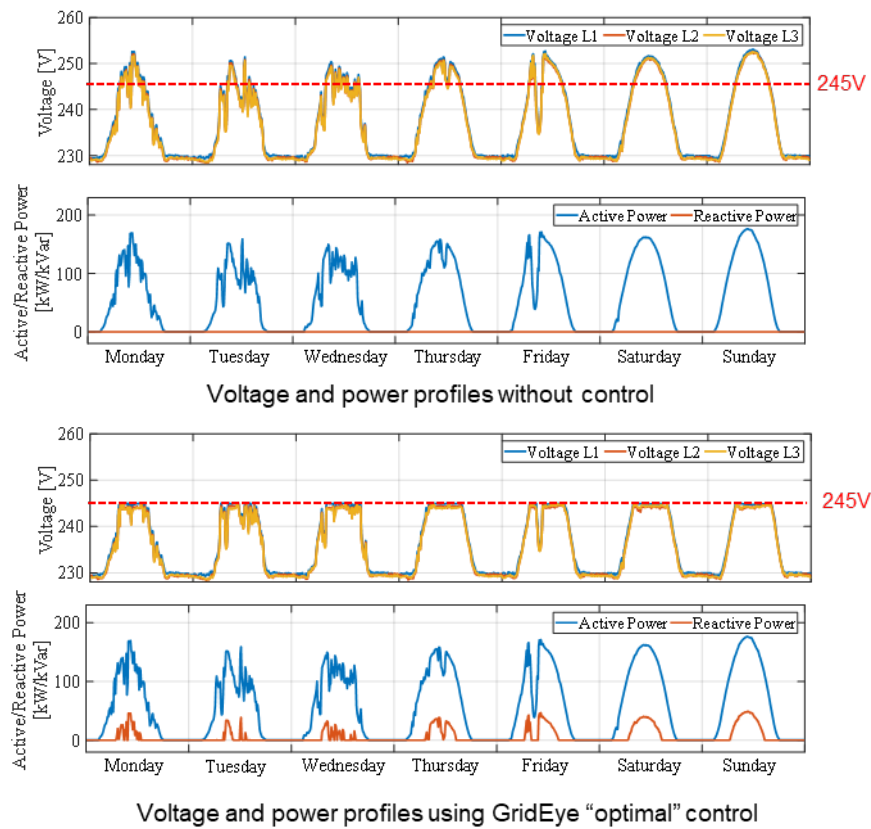
Figure 33 voltage profiles at node 2 as well as the PV inverters active and reactive power outputs for the case without control (top) and the case using the GridEye optimal control (bottom).

6 Conclusions

In this project, we studied both theoretical and practical aspects related to application of low voltage grid monitoring system on grid control and flexibility assessments.

In this respect, first we improved existing methods and algorithms developed in the scope of the previous SMILE project regarding computation of sensitivity coefficients of nodal voltages with respect to active and reactive power injections. The performed studies include i) analysis of the noise on GridEye measurements to validate the use of GLS method and ii) then proposing data filtering approach which effectively improves the method of sensitivity coefficient estimation.

Second, we have investigated the potential of using distributed PV plants for optimal voltage control considering the fairness of control actions. The voltage control is primarily formulated as a centralized optimization problem. Then, a distributed algorithm using dual de-composition framework is proposed. The performance of the control algorithms has been evaluated using the CIGRE LV benchmark grid. Both algorithms have successfully maintained the network voltage profile within safe limits. Even if the numerical analysis has shown that the distributed version of the algorithm requires a relatively large number of exchanged messages to converge, it does represent a useful solution when the state estimation output is asynchronous with respect to the controller actions.

Third, we investigated the Cybersecurity protection aspects the proposed low voltage monitoring solution. The example of DEPsys GridEye system was taken. During this activity a full threat model of the system was established, a risk analysis performed and a security architecture developed. The security architecture is based on a Virtual Private Network (VPN) which provides confidentiality and integrity of information exchanged between Smart Grid devices and backend infrastructure (back-end servers). This security architecture has been successfully tested and deployed in production. A penetration test has been performed on the backend infrastructure (including web-based frontend), on the infrastructure connecting modules as well as on the modules themselves. The result show that most critical risks identified at the beginning of the project were mitigated.

Forth, the methods of computation of voltage sensitivity coefficients with respect to active and reactive power injections are tested and validated under known operational conditions in the ReIne laboratory of HEIG-VD. The results of validation test shown that the relative differences between the sensitivity coefficients are good and testify the worthy performances of the model-less method.

Finally, we implemented and successfully tested a model-less and decentralized optimal control approach of DEPsys based on the estimated sensitivity coefficients, in a real distribution network in Switzerland.

7 Outlook

The theoretical and experimental results of the project demonstrate effectiveness of low voltage grid monitoring systems for advanced applications in operation and planning of low voltage distribution networks. Moreover, the results of the project show potentials of low voltage grids for provision of flexibilities (e.g., ancillary service such as voltage control). The project partners aim at further developing this direction of research with realistic industrial applications. In this respect, the next step is to develop appropriate control algorithms and an optimization framework for provision of ancillary services from low voltage grids toward upstream medium and high voltage grids. The control algorithms and the optimization framework shall consider not only the grid operational constraints (e.g., line's ampacity limits) bit also uncertainties associated with productions from distributed renewable energy sources.

8 Publications

- Numa Gueissaz, Konstantina Christakou, Jean-Yves Le Boudec, and Mario Paolone, "Fair Control of Distributed PV Plants in Low Voltage Grids", 2017 IEEE Innovative Smart Grid Technology Conference Europe, At Turin, Italy.

- J. Jaton, G. Besson, M. De Vivo, M. Carpita, M. Paolone, K. Christakou, C. Mugnier and O. Alizadeh-Mousavi, "Method for determining mutual voltage sensitivity coefficients between a plurality of measuring nodes of an electric power network". World Patent 182918, 26/10/2017.

- Mauro Carpita, Mokhtar Bozorg, Omid Alizadeh Mousavi, and Sebastien Westerlin, "Model-less/measurement-based computation of voltage sensitivities in unbalanced electrical distribution networks: experimental validation", Accepted to be presented in the 21st European Conference on Power Electronics and Applications (EPE'19 ECCE Europe), September 2019, Genova, Italy.

- Mauro Carpita, Jean-François Affolter, Mokhtar Bozorg, Douglas Houmard, and Sebastien Westerlin, "ReIne, a flexible laboratory for testing the low voltage networks", Accepted to be presented in the 21st European Conference on Power Electronics and Applications (EPE'19 ECCE Europe), September 2019, Genova, Italy.

9 Annex: ReIne laboratory – Distribution Grid Test Facility

9.1 Context and general information

With the challenges of the energy transition (development of renewable energies, phase-out of nuclear power and reduction of fossil sources) the electric network is changing. Among the changes, those linked with the low-voltage network are the following:

- Stronger penetration of the distributed generation
- Presence of active consumer, or *prosumers*
- Introduction and continuation of the opening of the electricity market
- Increase in telecommunication and control capabilities

These changes result in the arrival of intelligent network, more often called SmartGrids. This transition is not done instantly but over time, and to plan the upcoming evolution at best it is necessary to have test platforms in order to be able to test proposed solutions.

The ReIne laboratory (ReIne for *Réseau Intelligent*, French for smartgrid) is a platform that allows the emulation of a great number of different network topologies, in order to test smartgrid control methods as well as power electronic devices under various and controlled load and generation constraints [13].

Its principal characteristics are:

- Voltage level   230/400 V
- Topology   8 lines in a controllable matrix and a 9th that can be connected freely
- Type of line   emulated with discrete impedances
- Power   input transformer of 100 kVA
                       line nominal current of 145 A (100 kVA)
- Equipment   various load and generation devices, simulated or real
- Standard   NIBT 2015
- Control   centralized with a SCADA (Supervisory Control And Data Acquisition)
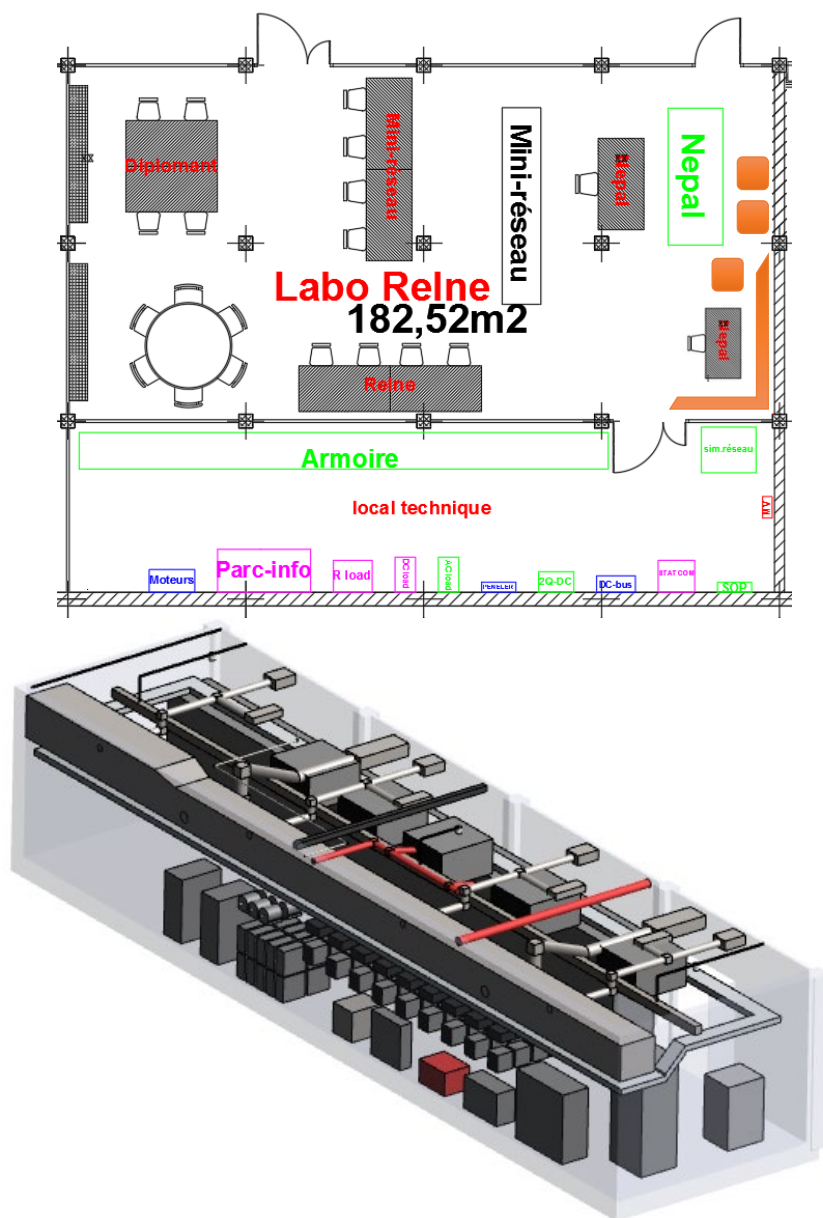- Uses   education and applied Research and Development

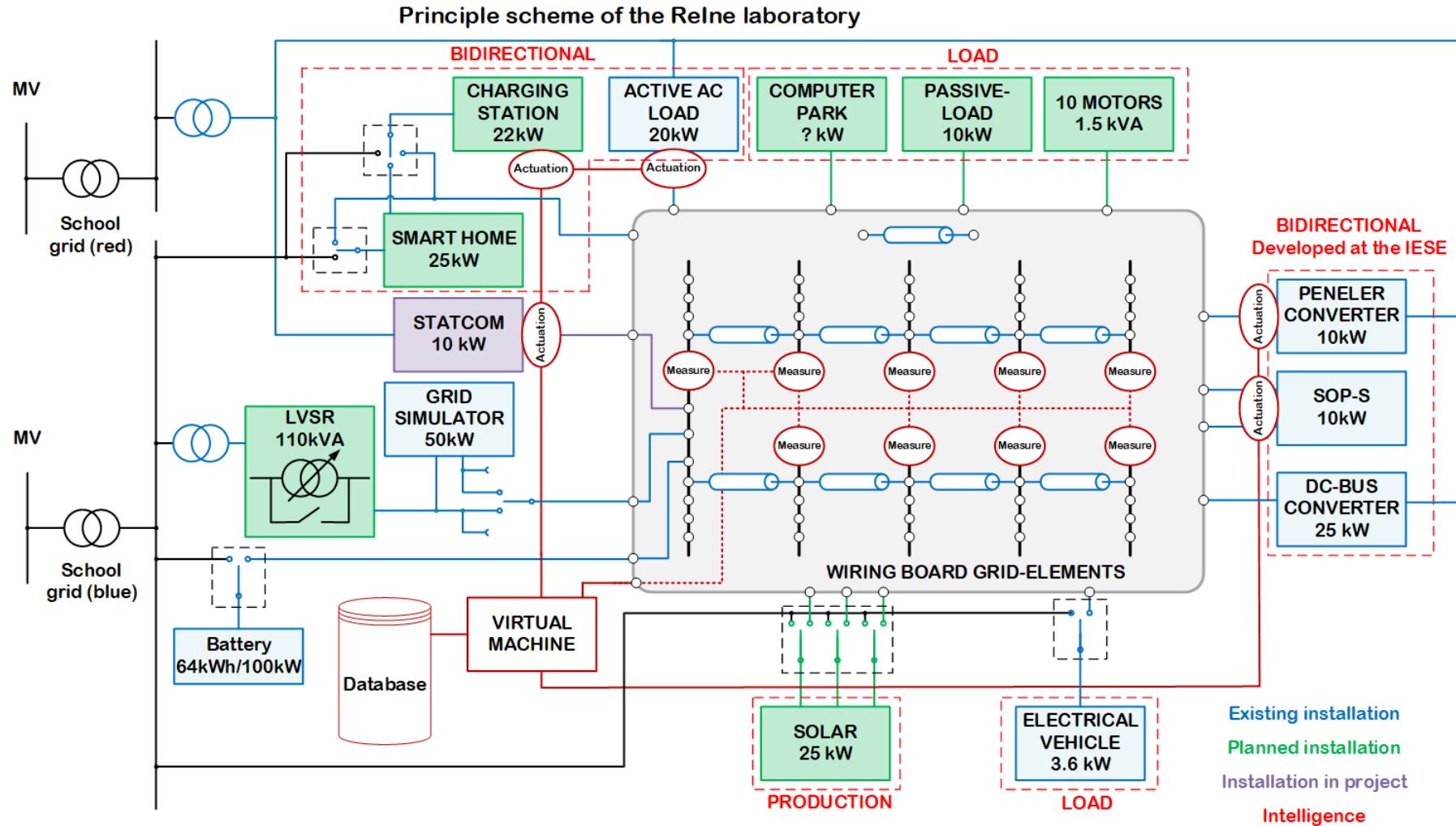Figure 34. Laboratory scheme and 3D view of the technical room

Figure 35. ReIne laboratory structure

9.2 Technical description

9.2.1 Overview

As we see in Figure 35, the laboratory is composed of a network on which it is possible to connect generation, passive and active loads, and bidirectional power electronic devices.

9.2.2 Modular network

Network synoptic

The network part of the laboratory is made of 8 lines positioned in a matrix and a 9th line that can be connected freely between two desired nodes (see Figure 36). Each line is emulated with discrete impedances.
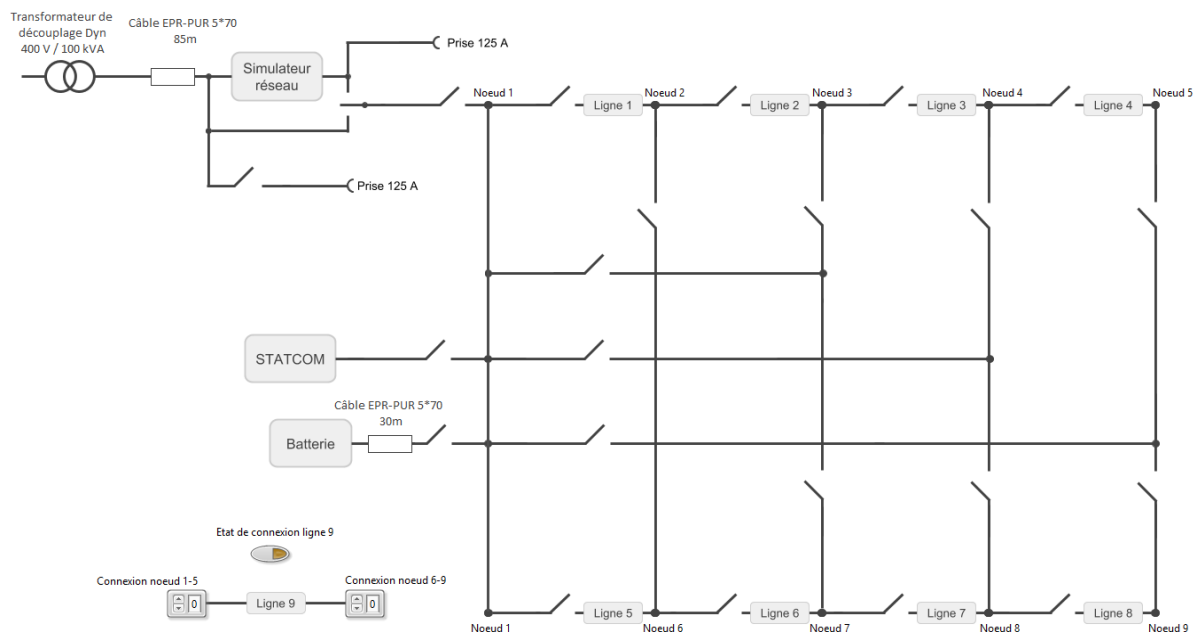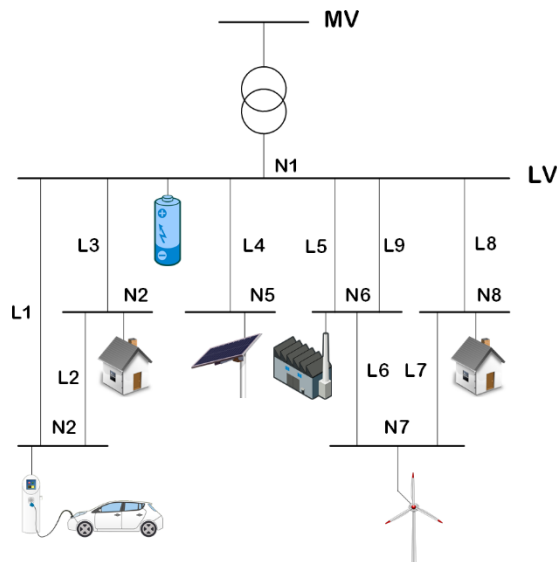

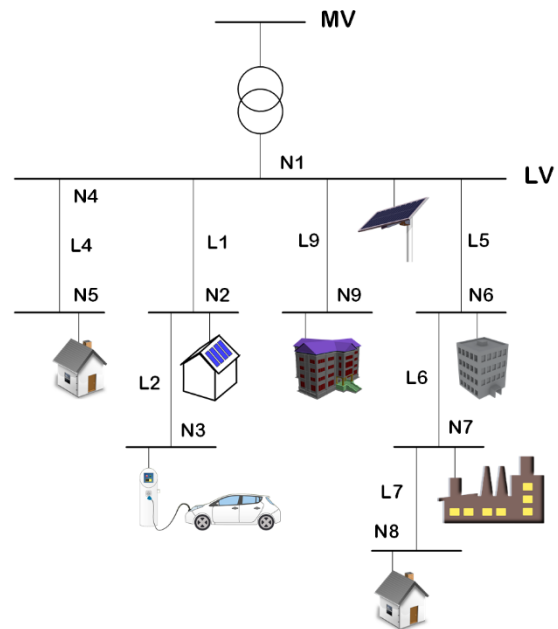Figure 36. Synoptic of the lines in the network

The configuration of the network to the chosen topology is made via the SCADA and is realized in a remote-controlled wiring board. This board also enable the users to connect all the different devices to the wanted node, every node being available (see Figure 37).
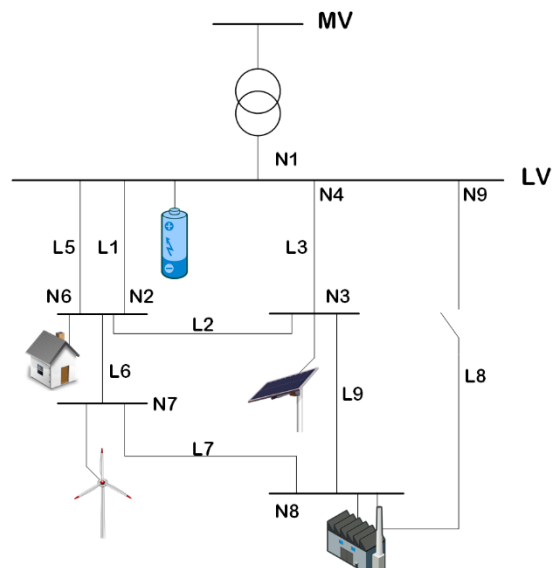
Figure 37. Examples of topologies that can be achieved with the 9 lines and the wiring board

Network elements characteristics

The characteristics of every element in the network are the following:

Network input transformer

Winding	Dyn11
Primary voltage	400 V
Secondary voltage	400 V
Short-circuit voltage	2.5 p.u.
Leakage inductance	1.2 p.u.
Copper losses	2083 W
Iron losses	808 W
Efficiency	97.19 %

Table 5 Characteristics of the network input transformer

Cable EPR-PUR 5x70

Linear resistance	Nominal voltage
0.272 Ω/km	1000 V

Table 6 Characteristics of the alimentation cable

Impedances of lines 1 - 9

module(Z)	phase(Z)	R	L	R/X
70 mΩ	73°	20 mΩ	215 µH	0.3

Table 7 . Characteristics of the emulated lines 1-9 at 50 Hz

9.2.3 Installations connected to the laboratory

Network simulator

It is possible to power the laboratory either with the school grid or through a network simulator 4-quadrant REGATRON *TopCon TC.ACS*. This simulator is made of two back-to-back multilevel converters that can generate a three-phase voltage in a big range of frequency, amplitude, unbalance and harmonic distortion. It is possible to give it a curve of parameters variations that the simulator will then follow, in order to test transient phenomenon.
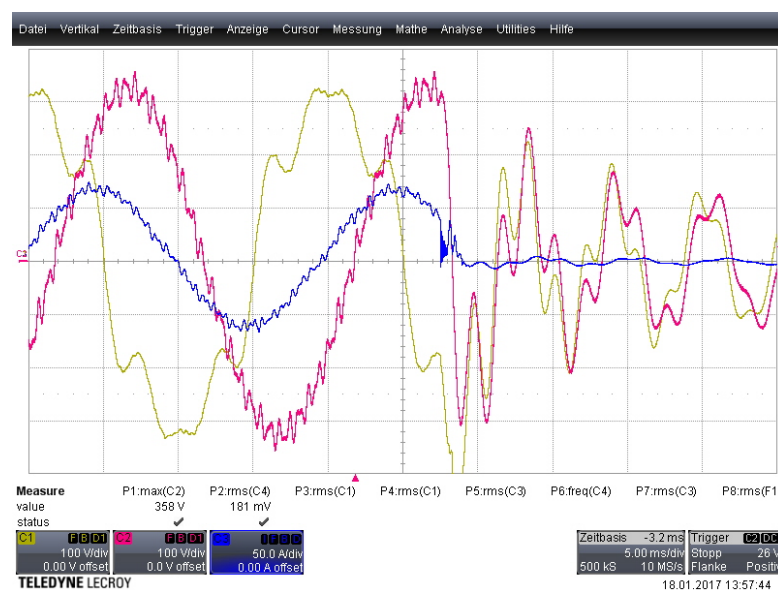

Figure 38. Example of a voltage profile obtained with the network simulator

Its main characteristics are the following:

REGATRON *TopCon TC.ACS*

Nominal power	50 kVA
Phase-neutral voltage	Up to 280 V
Nominal current	72 A
Frequency	Up to 1 kHz
Harmonics	Up to 5 kHz
Possibility to generate	Asymmetrical voltages Short-term failure Flicker Balanced or unbalanced voltage drop

Table 8 Characteristics of the TOPCON TC.ACS network simulator

It is planned to have a serial compensator between the input transformer and the network in order to modify the voltage at the point of coupling. The *LVRSys* 110 kVA from Sotero has been chosen.

Smart home

In addition to the network part, a smart home is also implemented in the laboratory. This installation is intended to be used in education but also for the test of industrial devices such as measurement devices (smart-meters for instance), performance tests on household appliances, system service strategy tests …etc.

The home is equipped in order to reproduce a real modern domestic load, with:

- A photovoltaic installation (a part of the panels of the solar carport with a converter *IMEON 3.6*)
- An AC battery for energy storage (*PowerLegato* from AUO)
- A water-heater that can be connected to the photovoltaic installation (*HeatMaster AP 207 CT*)
- A refrigerator-freezer (*TK80LA++* de Kibernetik)
- A dishwasher
- Cooking plates and one electric hoven

Batteries

In the framework of previous research projects, batteries were implemented at the HEIG-VD. These batteries can be connected to the ReIne laboratory at any node of the network.

TiRack **Leclanché storage with** *BAT100* **FeCon converter**

Capacity	63 kWh
Technology	Lithium-titanate
Converter power	120 kVA
Available active power	100 kW

Table 9 Characteristics of the storage system with batteries

Solar carport (charging station and solar generation)

A solar carport, i.e. a car shelter equipped with photovoltaic panels and with charging stations will be installed during fall 2018.

Figure 39. Solar carport and its charging station

A total of 85 solar panels Bisol 295 Wc will be installed. 12 are dedicated to the smart home production (i.e 3540 Wc) and the rest are connected to the laboratory via 3 three-phased converters, with the possibility to generate capacitive or inductive current.

The 3 converters are:

- SolarMax *TP2* of 5kVA associated with 3540 Wc of panels

- ABB *TRIO-8.5-TL-OUTD-S* of 8.5 kVA associated with 7375 Wc of panels

- Kaco *Powador 10.0 TL3 INT* of 9 kVA associated with 10325 Wc of panels

Below the carport, a charging station for electric vehicle GreenMotion *Private One* will be installed. It has an adjustable power between 3.7 and 22 kW.

AC Load

An electronic 4-quadrant load ENERGIA *EL20-AC* enables us to simulate a various type of loads or generation. It is thus possible to reproduce the behavior of the charging of an electric vehicle, an household's consumption, a wind turbine's generation or a solar power plant's generation.

EL20-AC

Nominal power	20 kVA
Nominal active power	18 kW
Phase-neutral voltage	25-277 V
Nominal current	25 A
Frequency	10-400 Hz
Harmonics	Up to 780 Hz

Table 10 Characteristics of the EL20-AC electronic load

It is planned to have passives loads in the laboratory but their specifications are not yet fixed.

Motors

A test bench of motors will also be present with 10 Siemens *1LA7096* asynchronous motors with a nominal power of 1.5 kW.

Devices developed at the IESE institute:

MMC Statcom

A MMC Statcom is in development within the IESE. It will be equipped with an energy storage thanks to a battery and has a nominal power of 10 kVA.

PENELER

PENELER is a DC/AC converter of 10 kVA developed from scratch in order to have a device to test modulation and control strategies.

SOPS

The Soft-Open-Point with Storage consist of two back-to-back converters based on the PENELER technology. They share a common DC bus on which we connect a battery through a DC/DC converter. This setup gives the possibility to transfer active power between two different lines of a network without

altering its characteristics, thus without increasing its short-circuit current and the need to modify its protection scheme. It can also support the voltage at both side with the injection of reactive power. Technical description and preliminary experimental tests of the SOPS are presented in [14].
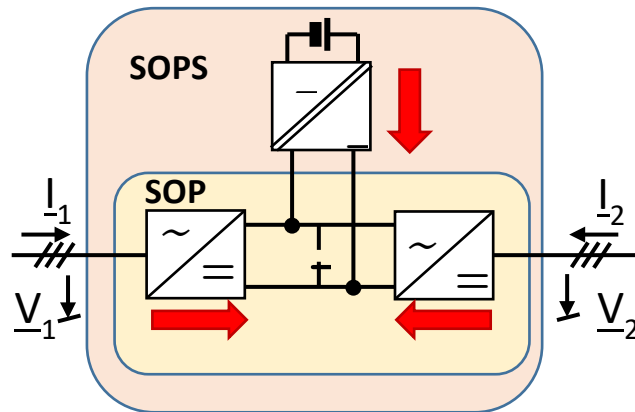

Figure 40. SOPS

DC-BUS

DC-BUS is an AC/DC converter for a microgrid DC bus demonstrator, targeted at energy distribution within a small residential building. Its nominal power is of 25 kW and various DC load can be connected to the main laboratory grid via this converter.

9.2.4 Network measurements

Measurements system for the SCADA

Every node and every line of the network (view Figure 36), as well as the connecting branches of every different devices are equipped with three-phased synchronous measurements.

Those measurements are made with National Instrument *cRIO-9035* modules, with:

- Sampling frequency of 50 kHz
- GPS synchronization

Therefore, it is possible to have the amplitude and the phases, but also the harmonic content of every voltage and current in the network.
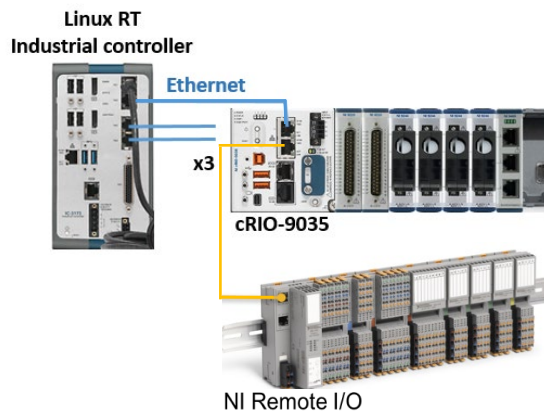
Figure 41. National Instrument measurement system

Those measurements are then clustered on a Real-Time industrial controller and sent to the PC that operates the SCADA. They can then be used for the test of various control algorithms.

Other measurements

Within the framework of another project, 5 *GridEye* devices from DEPsys are also dispatched in the network. They will be used as a secondary measurement system, using the functionalities proposed by DEPsys.

Figure 42. GridEye device from DEPsys

9.2.5 Supervisory Control And Data Acquisition (SCADA)

A SCADA written in LabView is implemented for the management of the entire laboratory, with the clustering of every measurements and the dispatch of the setpoints.

It can modify the topology of the network by controlling the contactors inside the wiring boards, start up the network and visualize the measurements with the possibility to record them. It is also planned to connect it to the different controllable devices of the laboratory (network simulator, electronic load, devices developed in the framework of other projects at the IESE) in order to send them setpoints.

This information clustering allows the implementation of high-level control strategies at the level of the entire grid, making it a smart grid.
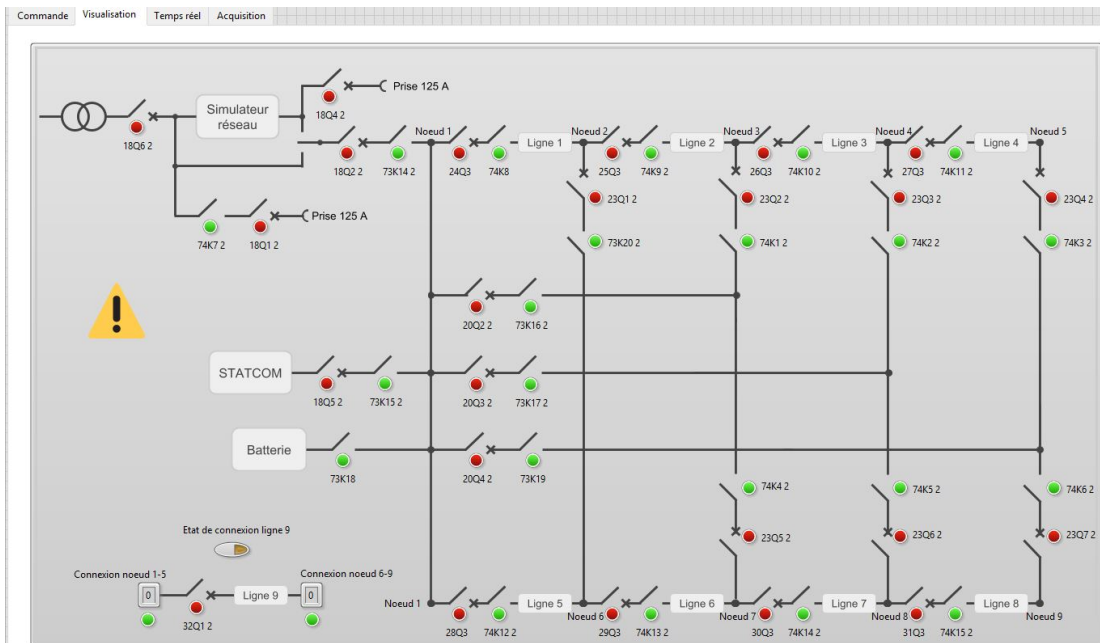
Figure 43. Snippet of the user interface of the SCADA

10 References

[1] C. Mugnier, K. Christakou, J. Jaton, M. D. Vivo, M. Carpita and M. Paolone, "Model-less/measurement-based computation of voltage sensitivities in unbalanced electrical distribution networks," in *Power Systems Computation Conference (PSCC)*, Genoa, Italy, 2016.

[2] J. Jaton, G. Besson, M. De Vivo, M. Carpita, M. Paolone, K. Christakou and C. Mugnier, "Method of determining mutual voltage sensitivity coefficients between plurality of measuring nodes of an electric power network". European Patent 16166721, 22 04 2016.

[3] J. Jaton, G. Besson, M. De Vivo, M. Carpita, M. Paolone, K. Christakou, C. Mugnier and O. Alizadeh-Mousavi, "Method for determining mutual voltage sensitivity coefficients between a plurality of measuring nodes of an electric power network". World Patent 182918, 26 10 2017.

[4] S. Papathanassiou, N. Hatziargyriou and K. Strunz, "A benchmark low voltage microgrid network," in *CIGRE symposium: power systems with dispersed generation*, 2005.

[5] J.-Y. L. Boudec, "Rate adaptation, congestion control and fairness: A tutorial," Available: http://ica1www.epfl.ch/PS files/LEB3132.pdf.

[6] K. Christakou, J. LeBoudec, M. Paolone and D.-C. Tomozei, "Efficient computation of sensitivity coefficients of node voltages and line currents in unbalanced radial electrical distribution networks," *IEEE Trans. Smart Grids,* pp. 741-750, 2013.

[7] D. P. Chiang and M. Palomar, "A tutorial on decomposition methods for network utility maximization," *IEEE Journal on Selected Areas in Communications,* vol. 24, pp. 1439-1451, 2006.

[8] N. Gueissaz, K. Christakou, J.-Y. L. Boudec and M. Paolone, "Fair Control of Distributed PV Plants in Low Voltage Grids," in *IEEE Innovative Smart Grid Technology Conference Europe*, Turin, Italy, 2017.

[9] J. B. Zhou Qiong, "Simplified calculation of voltage and loss sensitivity factors in distribution networks," in *16th Power System Computation Conference (PSCC)*, 2008.

[10] LEM, "LF 210-S," [Online]. Available: https://www.lem.com/sites/default/files/products_datasheets/lf_210-s.pdf. [Accessed 2018].

[11] N. Instrument, "NI-9220," [Online]. Available: http://www.ni.com/pdf/manuals/373920a_02.pdf. [Accessed 2018].

[12] N. Instrument, "NI-9467," [Online]. Available: http://www.ni.com/pdf/manuals/373230c.pdf. [Accessed 2018].

[13] M. Carpita, J.-F. Affolter and M. Capezzali, "Relever les défis de la transition énergétique," *Bulletin SEV/VSE,* pp. 39-43, 2018.

[14] F. Attanasio, S. Westerlain, T. Pidancier, M. Marchesoni, P. Favre-Perrod and M. Carpita, "Low Voltage Soft Open Point with Energy Storage: System Simulation and Prototype Preliminary Test Results," in *International Symposium on Power Electronics, Electrical Drives, Automation and Motion*, Amalfi, Italy, 2018.

[15] J.-Y. L. Boudec, Performance Evaluation of Computer and Communication Systems, Lausanne: EPFL Press, 2010.

[16] B. Schaffrin and A. Wieser, "On weighted total least-squares adjustment for linear regression," *Journal of Geodesy,* vol. 82(7), pp. 415-421, 2008.

[17] M. Pignati, M. Popovic, S. B. Andrade, R. Cherkaoui, D. Flores, J.-Y. L. Boudec, M. M. Maaz, M. Paolone, P. Romano and S. Sarri, "Real-time state estimation of the epfl-campus medium-

voltage grid by using pmus," in *Sixth Conference on Innovative Smart Grid Technologies (ISGT)*, 2015.

[18] M. Carpita, "SMILE-FA, "The theoretical and application Study on a Metering and Intelligent tool for Low Voltage grid control Enhancement – Flexibility Assessment"," HES-SO, Yverdon-les-bains, 2016.

[19] D. Roggo, "Compatibilité Electromagnétique entre réseaux intelligents et systèmes de production et de stockage," HES-SO, Sion, 2016.

[20] Commission International Electrotechnical, "IEC 61000-2-2:2002+AMD1:2017, "Electromagnetic compatibility (EMC) - Part 2-2: Environment - Compatibility levels for low-frequency conducted disturbances and signalling in public low-voltage power supply systems"," International Electrotechnical Commission, 2017-06-27.

[21] Commission International Electrotechnical, "IEC TS 61000-3-4:1998, "Electromagnetic compatibility (EMC) - Part 3-4: Limits - Limitation of emission of harmonic currents in low-voltage power supply systems for equipment with rated current greater than 16 A"," International Electrotechnical Commission, 1998.

[22] Regatron, "TopCon TC.ACS - Full 4-quadrant grid simulator," 2017. [Online]. Available: https://www.regatron.com/en/products-topcon/topcon-tc-acs.

[23] D. Roggo, "Bus-DC pour microgrid," HES-SO, Sion, 2015.

[24] J. A. Donenfeld, "WireGuard: Next Generation Kernel Network Tunnel," www.wireguard.com, -.

[25] J. Donenfeld, "WireGuard: Next Generation Kernel Network Tunnel," in *Proceedings of the Network and Distributed System Security Symposium (NDSS)*, 2017.